Supplementary Information

For Method-Dependent Variability in Hygroscopicity Parameter (κ) of Particles from Biomass-Burning Across Fuel Types and Burn Phases

Sara Aisyah Syafira[1,a], Dawei Hu[1], Aristeidis Voliotis[1,2], Huihui Wu[1,b], Osayomwanbor Ebenezer Oghama[1], Yunqi Shao[1], Sri Hapsari Budisulistiorini[3], Yu Wang[4], Michael Flynn[1], Peter James Gallimore[1,b], Hugh Coe[1,2], James Allan[1,2], and Gordon McFiggans[1]

Contents:

Supplementary Figures

Section 1. Supplementary Notes

Note S1. More Detailed Step-by-Step Error Propagation of HTDMA and CCNC

These are some of the error propagation rules used in this current study:

$$z = x + y;\ \sigma_z^2 = \sigma_x^2 + \sigma_y^2 \ldots . (1)$$

$$z = k \text{ x } x;\ \sigma_z = k\ x\ \sigma_x \ \ldots . . (2)$$

$$z = x \text{ x } y;\ (\frac{\sigma_z}{z})^2 = (\frac{\sigma_x}{x})^2 + (\frac{\sigma_y}{y})^2 \ \ldots (3)$$

$$z = \frac{x}{y};\ (\frac{\sigma_z}{z})^2 = (\frac{\sigma_x}{x})^2 + (\frac{\sigma_y}{y})^2 \ \ldots . (4)$$

For the HTDMA calculation, first error propagation was done following the hourly averaging formula, so the steps for each time duration interval will be:

(i) Numerator error propagation. In this first step, the 1st error propagation rule:

$$\sigma_z = \sqrt{\sigma_x^2 + \sigma_y^2}$$

was used by looping this equation through the entire data points, one by one.

(ii) Final error propagation. In this step, this 2nd rule was used:

$$\sigma_z = k\ x\ \sigma_x$$

The k value will be $\frac{1}{total\ number\ of\ the\ data\ points}$, whereas the σ_x is the propagated error obtained in the 1st step. The resulted σ_z in this step will then the final propagated error of each hourly mean κ value.

The above steps were conducted for each particle size. Therefore, each particle size has a set of data containing the hourly mean κ value of each time interval along with its propagated error. However, these collections of the HTDMA data were still going to pass through another process, which were the size number weighted mean κ calculation. Therefore, there would be 2nd error propagation according to the size number weighted mean κ calculation formula, following these steps.

(i) Repeated above step 1-2 for the hourly mean SMPS particle number error propagation

(ii) 2nd error propagation of the HTDMA data that contained these parallel steps:
   a.) Numerator error propagation using the 3rd and 1st error propagation rule
   b.) Denumerator error propagation using the 1st error propagation rule
   c.) Final error propagation using the 4th error propagation rule:

$$\sigma_z = z\sqrt{(\frac{\sigma_x}{x})^2 + (\frac{\sigma_y}{y})^2}$$

For the CCNC calculation, there was only one error propagation that follow the hourly averaging formula as in the 1st error propagation step of HTDMA data that contained two steps 1st error propagation rule and 2nd error propagation in series.

For the chemical-based κ values prediction, the two steps error propagation as in the CCNC error propagation and the 1st stage HTDMA error propagation was applied while applying the hourly averaging to each of the component instruments, i.e. SP2 and AMS, specifically to each of the AMS organic data, Chl data, SO4 data, NO3 data, and NH4 data. The second error propagation will be several steps of error propagation following the detailed chemical composition-based κ prediction equation that used the 1st, 2nd, and 4th rules.

Note S2. Explanatory Overview of the Different Approaches in Chemical-Composition-based-Hygroscopicity Prediction

Generally, the prediction formula is based on the basic theory particle mixing equation:

$$\kappa = \sum_i \varepsilon_i \kappa_i$$

where ε_i is volume fraction, and κ_i is hygroscopicity of fraction i. In general, the fractions were consisted of organic fraction and inorganic fractions (in the form of neutral salts) with known κ values used as the inputs, as described by Gysel et al (2007).

Different approaches to using this formula arise from varying assumptions aimed at simplifying calculations based on the chemical composition data provided by instrumental measurements. The first group of approaches uses volume fractions as the relative amount of each component in the prediction calculations. The second group uses mass fractions instead of volume fractions, operating under the assumption that each particle component has similar density to the overall particle density (Che, H. C. et al. 2017). Kim N et al (2017) compared κ values obtained from the HTDMA measurements and three different methods for the chemical composition-based κ prediction calculations, as referenced in the literature. Of these methods, two used the volume fraction approaches and one used the mass fraction approach. The results indicated that one of the volume fraction approaches resulted in predictions that had better agreement with the measured values, i.e. had closer values of the measured-to-predicted κ values ratio to 1, compared to the mass fraction approach, with the delta measured-to-predicted κ ratio between these two approaches were as much as 0.10-0.24. The other volume fraction was 0.04-0.08 less accurate than the mass fraction approach. The difference between the first and second volume fraction approaches was the choice of organic κ values. Both approaches used same single inorganic ion pairing algorithm and the same referenced κ and density values for inorganic salts. When the second volume fraction approach was improved by including BC, the calculated measured-to-predicted κ ratio improved, aligning closer with the first volume fraction approach.

As briefly introduced earlier, another difference among the approaches lies in whether BC is included as a separate component fraction of the particles in addition to inorganic and organic compounds. Some studies, such as those by Kim, N. et al. (2017), Fan, X. et al. (2020), Healy et al. (2014), and Li, C., et al (2016) included BC as a distinct fraction with hygroscopicity value assumed to be zero. Other studies excluded BC (Reilly and Wood 1969 in Gysel et al 2007; Chang et al 2010; Kim N et al 2017; Che, H. C. et al 2017; Gunthe, at al., 2009; Pohkler, M. L., et al 2023) likely assuming its content to be negligible in certain ambient environments.

As mentioned earlier, the research by Kim N et al (2017) showed that including BC into the total particle fraction improved the agreement between HTDMA-measured κ and chemical

composition-based predicted κ. Specifically, this inclusion resulted in higher correlation (r=0.6 compared to r=0.45) and reduced variability in the ratio between measured and predicted values (1.23 ±0.26 compared to 1.35± 0.35) when applied to urban aerosols.

However, another study took a different approach by incorporating BC fraction into the organic fraction rather than treating it as a separate fraction outside the inorganic and organic fractions. Li et al. (2016) explained this method by suggesting that any additional effects of BC, e.g. particle restructuring, could be directly merged or reflected from any deviations in the calculated organic κ values from their expected values when BC is included within the organic fraction. This approach could have possibly benefited their analysis to be more practically simpler since they did not actually measure both the OC and BC contents directly in parallel with two different parallel measurements. Instead, they used a thermal-optical transmittance OC/EC analyzer that measure carbonaceous materials containing both OC and EC that provided separated data of OC fractions at different temperature, OP (pyrolyzed carbonaceous component) and three EC fractions at different temperatures through a certain protocol and procedure.

To provide either organic or inorganic fractions, most studies relied on online chemical composition measurements using AMS. However, some studies employed offline particle filter chemical composition measurements. For use in prediction calculations, many researchers used the single ion pairing algorithm introduced by Reilly and Wood (1969) to convert inorganic ion data into neutral salts data. These conversions typically referenced well-characterised inorganic salts with known hygroscopicity and density values (Topping et al 2005). Alternatively, some studies—especially those using mass fraction approaches instead of volume fraction—used a constant inorganic κ value of 0.6 (Che, H. C. et al. 2017; Gunthe et al 2009). In these cases, all inorganic ions usually detected by AMS, such as ammonium, nitrate, sulphate, (Gunthe et al 2009) and chloride (Pohkler, M. L. et al. 2023) were directly summed as the total inorganic mass and assumed to have κ of 0.6. This method did not require a single ion pairing algorithm, since all ions were presumed to form similar inorganic neutral salts with similar hygroscopicity and particle density.

For the organic κ values, some researchers used a fixed value, such as 0.1 (Gysel et al 2007; Che, H. C. et al. 2017; Gunthe et al 2009) or a range between 0.1-0.15 (Duplissy et al 2011; Levin et al 2014; Wu et al 2016) as referenced in (Kim, N. et al 2017). However, this simplification does not fully capture the diversity of organic compounds present in aerosol particles in the world, which can exhibit a slightly wider range of κ . For example, Pohkler *et al* (2023) noted that laboratory-derived organic κ values range from approximately 0.02 to 0.4, but field-measured organic κ values κ_{org} range from 0.04 to 0.25.

Owing to possible variability, some studies opted to use non-constant organic κ values derived from experimental findings. These values were calculated using linear regression equations that corelated organic κ values with the oxidation level of particles, showed by metrics such as the O:C ratio value or f44. (Kim N et al 2017; Chang et al 2010; Fan X et al, 2020; Healy et al 2014). For instance, Kim et al. (2017) applied the regression linear equation κ_{org} = 0.29±0.05(O/C). In another study, the κ_{org} - O/C ratio correlation equation is κ_{org} = 0.19 (O:C)−0.03 (Wu, Z. J., et al, 2013). However, these approaches often resulted in overestimated predicted κ values compared to HTDMA-measured κ values. Plotting O/C ratio against organic κ values recalculated from the difference between overall κ_{HTDMA} and the sum of the fractional

κ contributions weighted by volume fraction, Kim et al. (2017) found a lower gradient (0.1 instead of 0.29 or 0.19) in the linear regression equation. Despite this adjustment, the correlation coefficient remained very low (r<0.2), aligning with conclusions from other studies (Wu et al 2016; Rickards et al 2013) that oxidation state alone does not determine κ_{org}.

Note S3: Further information or explanation about the HTDMA and CCNC graphs in Figure 3 and Figure 4

The data is displayed in two plots. First is the box-and-whisker plots illustrating the range or distribution of the whole population of the measured hourly averaged hygroscopicity values across all experiments. Second is the scatter plots with propagated error bars to illustrate the 1-hour variability of each hourly mean hygroscopicity value. In the plausibility check, however, the error bars are not propagated errors. Instead, they reflect the minimum and maximum values of the hourly mean hygroscopicity calculated using the minimum and maximum extended fractional κ values, respectively

In the box plots, the horizontal middle line within each box represents the median (50^{th} percentile, q2). The top and bottom edges of the boxes indicate the 75^{th} (q3) and 25^{th} percentiles (q1), respectively. Whiskers extend to the maximum and minimum values that are not outliers, defined as q3 + 1.5 * (q3-q1) for the upper limit and q1 - 1.5 * (q3-q1) for the lower limit. Data points outside the whisker lines are considered outliers and are shown as dots. Notches in the box plots represent the range $q_2 - 1.57(q_3 - q_1)/\mathrm{sqrt}(n)$ and $q_2 + 1.57(q_3 - q_1)/\mathrm{sqrt}(n)$, where n is the number of valid observations, without any NaN values, as per Matlab Documentation.

More Explanation to the HTDMA graph (**Figure 3**)

The **right-side panels** of **Figure 3** (3.a.(ii) and 3.b.(ii)) present scatter plots comparing paired values of hourly mean predicted κ and hourly size-number-weighted averaged measured κ across all the different experiment types. The corresponding **left-side panels** (3.a.(i) and 3.b.(i) show box-and-whisker plots illustrating the distribution of hourly averaged κ values of both measured and predicted data for each experiment type. These data points were collected across multiple repetitions and aging stages, including dark aging and pre-aging, representing fresh emission. Therefore, the box-and-whisker plots demonstrate the variability in κ values across both repetitions and aging conditions. The time series plots of the points were displayed in Figure S4.

The vertical error bars in **Figure 3.a.(ii)** and **Figure 3.b.(ii)** represent propagated errors, combining three elements: initial unaveraged κ value errors from graph fitting or raw data processing, the standard deviation of hourly variability, and size-dependent variability. More detailed explanation in the Methods section and Supplementary Information, Note S1. The horizontal error bars in **Figure 3.a.(ii)** show propagated errors from the chemical composition-based predicted κ values derived using component κ values of 0.1 for organic κ and 0.6 for inorganic κ. In **Figure 3.b.(ii),** the same data points are shown, but instead of showing propagated errors, the error bars reflect predicted κ values that were calculated using the minimum and maximum values of the varied, rather than single, fixed component κ values.. The minimum values used were: BC κ = -0.05, inorganic κ = 0.4, organic κ = 0.05. The maximum values used were: BC κ = 0, inorganic κ = 0.8, organic κ = 0.15.

Note S4: Further discussion about the detailed patterns, error bars, and outlier investigation of HTDMA-derived κ values

Notably, the peat experiment, which produced smouldering-type smoke, had HTDMA-measured κ values closely aligned with those of flaming hardwood–both representing the lowest κ values. In contrast, flaming softwood exhibited the highest range and median HTDMA-measured κ values. The κ values for the other three experiment types fell between those of the three aforementioned experiment types. Flaming softwood had higher averaged HTDMA-measured κ values than flaming of hardwood, while smoldering softwood similarly had higher averages compared to smoldering of hardwood.

Some data points from the peat experiment had larger HTDMA-measured κ error bars compared to others. Upon closer inspection, the large error bars for peat data points were not caused by curve-fitting errors but rather the high variability of data points within the one-hour interval. Screenshots of graph fitting for these data points, which demonstrate the large, propagated errors, are provided in Figure S5.

An upper outlier in the flaming softwood experiment appeared consistently in the box-and-whisker plots for both the measured and predicted κ values. This consistency suggests that the outlier was likely not merely a result of measurement errors and may represent valid data points with potential scientific significance–possibly reflecting a specific reason for the sudden increase in κ. It could probably be due to its highest inorganic fraction at around 0.12 compared to the other data points of this flaming hardwood experiment. In contrast, outliers in the HTDMA-measured mean κ from other experiments did not have corresponding predicted value outliers. This discrepancy suggests that those outliers can be excluded from subsequent analyses to enhance accuracy. Nonetheless, these outliers are still included in the scatter plots in **Figure 3.a.(ii)** and **Figure 3.b.(ii).**

Note S5: Further case-by-case discussion of SPAR curves from Externally Mixed Particles and the Processing

The differences among the derived κ values from the three approaches, i.e. two direct measurements and one chemical composition-based prediction will firstly be influenced by both the presence or absence of external mixture and the tested particle sizes of each approach, especially for the non-size-resolved approaches of both the prediction and the CCNc measurement. As in this current study, the κ prediction was done for bulk composition of the whole polydisperse aerosol particles, ranging from the instruments' minimum to maximum measurement range. It is about similar for the CCNc measurement, which also measures the bulk particles. In non-size-resolved CCNC measurements, the derived κ value reflects the effective hygroscopicity of the particle population activating at the critical diameter (D_{50}), not the intrinsic κ of particles exactly at D_{50}.

The absence of external mixtures containing particles with distinct chemical compositions and hygroscopicities—especially when these differences are not distributed uniformly across the scanned particle sizes—will likely result in better agreement between bulk chemical composition-based κ predictions and size-resolved CCNc-measured κ values. However, if such external mixtures are present, this agreement can be affected. In this case, the match between predicted and measured κ values depends strongly on the appropriateness of the selected effective supersaturation (SSeff), which is related to the measured D_{50}. This D_{50} should ideally correspond to the mean, median, or mode of the particle size distribution used for the κ prediction from bulk chemical composition.

A first example of this complexity arises when hygroscopicity varies with particle size. For instance, if smaller particles are more hygroscopic than larger ones, the CCNc-derived κ—based on the activation fraction (AF) curve—will represent more of these smaller, more hygroscopic particles. Meanwhile, bulk composition-based predictions (e.g., from AMS-SP2 data) might be biased toward larger, less hygroscopic particles, leading to a predicted κ value that is lower than the CCNC measured one. This results in a low predicted-to-measured κ ratio. Using a κ value based on a weighted average across different size-dependent hygroscopic modes—essentially an averaging line between the peaks—can help reconcile this difference by capturing the overall hygroscopicity more accurately. Conversely, there could be hygroscopicity increases as the particle sizes increase. In this case, CCNc-measured κ value can be underestimated relative to the true κ value of the more hygroscopic particles (which dominate the mass or chemical signal in SP2-AMS measurement), because the small, less hygroscopic particles delay the activation onset in the AF curve, artificially increasing the D_{50}. This results in a higher predicted-to-measured κ ratio.

Additionally, the presence of nearly hydrophobic particles could also affect the derived CCNc κ values. Small hygroscopicity of the nearly hydrophobic particles could appear in the SPAR curve as ramp increases in the AF fraction values at large sizes instead of plateauing after achieving the steep AF increase. With the widely used fitting parameterization, the captured hygroscopicity value only reflects the hygroscopicity of the hygroscopic particles without including the nearly hydrophobic particles. Tao, J., et al (2020) proposed an improved parameterization scheme that produces six parameters representing the number fraction, the average activation diameter, and activation diameter deviation for both apparently hygroscopic particles and nearly hydrophobic particles. However, applying this scheme is likely not straightforward when the measured AF data points show unusual shape at which continuous

decreases in the AF values appear after achieving the steep increase and maximum AF, as mostly shown by the measured data points of the current biomass burning experiments that different to the SPAR curves of Tao J et al (2020) Figure 2(c).

Note S6: Other (data processing related) factors affecting the resulting CCNc κ

Several factors can influence the derived hygroscopicity values from the CCNC measurements, and consequently, the predicted-to-measurement κ ratio. Among these factors is the choice of parameterization scheme. Commonly used schemes include the formula by Rose et al (2008), which is widely adopted and recommended by Tao et al (2018); the power function formula (Meng et al 2014; Padro et al 2012); and the exponent formula (Deng et al 2013). All three parameterization schemes have been shown to fit well with the activation ratio (AR) sigmoid-shaped curves, also known also as SPAR (Size Particle Activation Ratio), and consistently use CCNC-related activity parameters such as midpoint activation diameter (Da), CCN fraction, and hygroscopicity heterogeneity (Tao, J., et al 2018). A key challenge arises when CCNC measurements of complex aerosol complex mixtures in non-single sigmoid-fitted curves. These curves often exhibit multiple activation regions unrelated to double charging (Vu, D, et al 2019, Figure 2). The height and length of the asymptote–the plateau between the first and second activation–depend on the relative fraction of the two externally mixed particles and the hygroscopicity of each particle population. Non-hygrosopic particles are identified by a maximum activation fraction less than one. Vu, et al. (2019) systematically demonstrated in laboratory examinations that separating and processing the different activation parts of a multiple activation curve for a known mixture resulted in a good agreement with single values obtained from each compound tested separately. Additionally, concerns have been raosed about the effect of nearly hydrophobic particles—those activated only at very large particle size, can bias the calculated hygroscopicity. To address this, Tao et al. (2020) proposed an improved parameterization scheme originally proposed by Rose et al (2008). This improved scheme increased the agreement between the activated fraction (fa) derived from CCNC measurements and that from HTDMA data. It also increased the size-resolved hygroscopicity parameter for particles smaller than 100 nm, providing a better fit to the CCNC-measured SPAR curve (Figure 1 Tao J, et al 2020).

In this study, no individual sigmoid fittings or separate activation analysis of SPAR CCNC measurement curves were conducted. Instead, the original scheme by Deng et al. (2013) was applied with curve-by-curve adjustments based on visual observations to address potential instrument spikes or excessively low particle concentrations. Unlike the CCNC measurement graphs in (Tao, J., et al 2020), which showed a ramp-like increase at larger particle sizes followed a steep initial increase, many of the CCNC measurement curves in this study resembled those in Vu, et al. (2019, Figure 8). These curves displayed a decreasing trend at larger particle sizes. This decrease was attributed to the presence of non-hygroscopic ($\kappa = 0 – 0.001$) yet wettable species such as BC, which suppresses the total hygroscopicity of the aerosol population at large particle sizes. BC's dry particle size distribution generally peaks at larger particle sizes than other aerosol types, and its pure form activates as cloud droplets only at particle sizes around 250 nm (Vu, D., et al 2019). In an external mixture containing highly hygroscopic particles, such as Na_2SO_4, and BC, the SPAR curve initially shows a steep increase at smaller sizes. This steep increase reflects the activation of the highly hygroscopic fraction, which typically correlated with a smaller dry particle size distribution than that of BC. The curve then transitions into a decreasing trend, followed by a stagnant or slightly increasing end as BC particles begin to activate (Vu, D., et al 2019). When BC is mixed with less hygroscopic particles, the SPAR curve displays a less steep increase at moderately small dry particle sizes.

This may include single or multiple activation regions before the start of the decreasing trend caused by BC and nearly hydrophobic BC-containing particles (Vu, D., et al 2019). Furthermore, a SPAR curve with a non-decreasing end (and a maximum F_A less than 1) may arise from an external mixture containing non-hygroscopic or non-activated particles if the dry particle size distributions of the mixture's aerosol population fractions are approximately similar.

The curve-by-curve adjustments applied to the CCNC SPAR curve fittings in this study were as follows:

i) The maximum activation fraction (F_A) was fitted to the highest peak of the data points, ignoring the decreasing trend observed at larger particle sizes.
ii) For data exhibiting two peaks (e.g., an initial lower FA peak followed by a higher peak), the slope wwas adjusted to represent average between the two peaks, rather than strictly fitting the slope of the highest peak.
iii) The starting data point was chosen as the first points with minimal fluctuation or with nearly or decreasing to zero. The ending data point was selected at the highest peak, ignoring any subsequent decrease in data points at larger sizes.
iv) Particle size distribution graphs were reviewed to identify and exclude anomalous or "suddenly jumping" data points.

Examples of these curve fittings are provided in Figure S7. Different SS values produced varying hygroscopicity, especially at low SS (<0.1%) compared to higher SS values. Separate plots of the data points at different SS values, including scatter plots and box-whisker plots, are shown in Figure S8. As mentioned earlier, the experiment dates used for CCNC-measured versus predicted data can be found in Table S2. Although the same experiment dates were chosen for SS values of 0.1%, 0.3%, and 0.5-0.6%, the κ variability for each fuel type at each SS value differed. Special caution should be applied to data at SS = 0.1%, given that variability at SSeff < 0.1% exceeds 40%. (Rose, D et al, 2008). Additionally, research has shown that CCN counter has kinetic limitations for droplet growth at low supersaturation (SS < 0.1%), leading to underestimation of hygroscopicity (Tao, J et al, 2023). Based on Figure S8, the measured CCNC κ values for different fuel type tested at 0.0965% and 0.1322%, grouped under SS = 0.1%, did not always show lower values compared to those measured at higher supersaturation values. These results suggest that the low supersaturation kinetic limitations may have had a lesser impact on these specific data points. Trends in the median values of CCNC κ values with increasing SS values (from 0.1% to 0.5-0.6%) fluctuated and varied by fuel type. Between SS = 0.8% and 1%, the changes also differed across fuel types. Scatter plots of separated data points for each SS value, as shown in Figure S8, indicate that the data set for the lowest SS contained more averaged data points with large propagated errors. This may suggest that higher SS values in this study resulted in either (i) more stable and reliable measurement that better fitted the sigmoid curve fitting, or (ii) less fluctuation or evolution of hygroscopicity during the one-hour averaging interval, or combination of both.

Other factor that could affect –in just probably immeasurably small portion, the resulting CCNC hygroscopicity, represented as κ values, is the choice of the Kohler models used to derive the κ values. As widely known, Kohler theory equation has its most basic form as below:

$$s = a_w \,.\, Ke \;;$$

at which a_w is water activity following Raoult's law effect and Ke is Kelvin curvature effect factor with the most basic or widely known description of the Ke is as below:

$$Ke = \exp\left(\frac{4\sigma_{sol}M_w}{RT\rho_w D_{wet}}\right)$$

However, the available formulas in determining either mostly a_w value or Ke can be varied as listed and detailed by Rose et al. (2008) in its Appendix section resulting in several versions of Kohler theory equation formula that those formulas could either or not contain κ parameter – a parameter that was closely linked to the a_w part.

Among the available formulas, an activity parameterization (AP) model introduce Kohler theory equation as below:

$$s = a_w \exp\left(\frac{4\sigma_{sol}M_w}{\rho_w RT g_s D_s}\right)$$

Another model, which is osmotic coefficient (OS) models introduced the a_w formula as below:

$$a_w = \exp\left(-v_s\Phi_s\mu_s M_w\right)$$

Meanwhile, Van't Hoff factor (VH) models based its a_w value through this formula:

$$a_w = \frac{n_w}{n_w + i_s n_s} = \left(1 + i_s\frac{n_s}{n_w}\right)^{-1} = (1 + i_s\mu_s M_w)^{-1}$$

So that the following Kohler theory equation formula as below:

$$s = \exp\left(\frac{A}{D_{wet}} - \frac{B}{D_{wet}^3}\right)$$

with the value of A and B are as below:

$$A = \frac{4\sigma_w M_w}{\rho_w RT};\ B = \frac{6i_s m_s M_w}{\pi M_s \rho_w} = \frac{i_s M_w \rho_s D_s^3}{M_s \rho_w} = \frac{6i_s n_s M_w}{\pi\rho_w}$$

A model that introduced and directly include the a_w value contributing composition dependent hygroscopicity parameter κ as used in this current research is the effective hygroscopicity (EH) parameter model that the a_w - κ relationship was defined as:

$$a_w = \left(1 + \kappa\frac{V_s}{V_w}\right)^{-1}$$

resulting in the Kohler equation theory formula that used in this current research as below:

$$s = \frac{D_{wet}^3 - D_s^3}{D_{wet}^3 - D_s^3(1-\kappa)}\exp\left(\frac{4\sigma_{sol}M_w}{RT\rho_w D_{wet}}\right)$$

There is another model that directly correlate sc with κ while most of other Kohler theory models including the above equation compute the s values until a maximum value is reached to be noted as the particles' crtical supersaturation value. That model is Analytical approximation (AA) model with formula described as below:

$$s_c = \exp\left(\sqrt{\frac{4A^3}{27\kappa D_s^3}}\right)$$

with A value $\approx (0.66 \times 10^{-6}\ K\ m)/T$ is inserted as the Kelvin term parameter

As compared in Rose et al. (2008), along with the available choices of the CCN SPAR curves parameterization schemes, the chosen Kohler models can play an important role in ensuring comparability of hygroscopicity values across studies without bias. The comparative study by Rose et al. (2008) showed that differences in approaches for deriving κ values, i.e. variations in thermodynamic parameterization schemes and Kohler models, could produce relative deviations up to 12% for NaCl and 25% for $(NH_4)_2SO_4$. However, the current study used only one type of both the CCN SPAR curve parameterization scheme and the Kohler theory based hygroscopicity parameter (κ) formula highlited in the Method sectionfor the entire

experiment. This approach eliminates deviations related to the variability regarding these factors, ensuring uniformity in the resulting κ values.

To conclude, the variability of the hourly mean CCNC-measured κ values showed significant dependence on the SS applied during the measurements. The error bars reflected how well the applied sigmoid curve fit the measured data, incorporating the one-hour variability in the propagation process. Instrumental measurement uncertainty, such as the relative deviation of less than 10% for SS > 0.1% as reported by Rose et al. (2008), was not accommodated or propagated in this study. However, this contribution is relatively minor compared to other sources of error, such as the D50 error or hourly variability or standard deviation, and is unlikely to substantially affect the calculated propagated errors.

Another factor that could possibly influence the CCNC κ values thus their differences with predicted values are –in this current study, the exclusion of the non externally mixed non hygroscopic particles. In the AMS-SP2 chemical composition based bulk κ prediction calculation, no distinction between pure BC particles and BC containing particles. Therefore, presence of externally mixed pure BC can lead to lower predicted to measured κ values ratio. This was beacuse the CCNc measurement ignore the non hygroscopicic particles in the averaged values of the measured bulk κ values, while the pure non hygroscopic values in the prediction can contribute in lowering the overall, i.e. averaged bulk predicted κ values. This could probably have been solved by excluding the BC data that has no coating thickness, but not yet applied in this current study. The graphs of the maximum activation fraction AF of each experiment was in Figure S10

Notes S7: Additional Notes of the Discrepancy Factors' Investigation

S7.1 Role of propagated uncertainty and within-experiment variability in interpreting κ discrepancies

The discrepancy analysis in this study focuses on mean or median κ values across experiment types. This choice is intentional and reflects the need to distinguish systematic, method-related effects from intrinsic experiment-specific variability. Interpretation of κ discrepancies, therefore, requires consideration of how uncertainty and variability are sampled and propagated by each κ-determination approach.

For CCNC-derived κ values, propagated uncertainty is dominated by the determination of the activation diameter (D_{50}) from size-resolved particle activation ratio (SPAR) curves. Small uncertainties in D_{50} can translate into large κ uncertainties, particularly at low effective supersaturation. As a result, CCNC κ uncertainties reflect a combination of SPAR curve-fitting sensitivity, hour-to-hour variability, and supersaturation-dependent behaviour, rather than purely atmospheric variability. Despite this, the majority of hourly mean CCNC-derived κ values exhibited apositive offset relative to composition-based predictions across experiment types (Figure 4(a.ii) and 4(b.ii)), indicating that the observed offset cannot be explained by uncertainty alone. As a reminder, values from different supersaturation levels are not averaged; they are aggregated.
In contrast, the uncertainty structure of HTDMA-derived κ values is dominated by within-hour variability and particle-to-particle heterogeneity under subsaturated conditions. Propagated errors primarily reflect variability in measured growth factors across the selected particle sizes, rather than fitting uncertainty. The absence of a consistent directional offset relative to predicted κ values, together with pronounced fuel- and burn-phase-dependent variability,

indicates that non-systematic, experiment-specific factors dominate the HTDMA uncertainty structure.

κ values predicted from AMS–SP2 chemical composition exhibit comparatively narrow uncertainty ranges. This behaviour reflects temporal averaging, mass-weighted representation of the aerosol population, and the use of uniform component κ assumptions, rather than reduced physical variability. Consequently, predicted κ values provide a stable reference for identifying systematic discrepancies, while not capturing the full extent of variability observed in direct measurements.

Taken together, the distinct uncertainty and variability structures associated with CCNC, HTDMA, and composition-based κ determination justify the use of mean or median κ values for inter-method comparison and demonstrate that κ discrepancies cannot be interpreted without explicit consideration of method-specific uncertainty propagation. As a note, median values are observed when making comparisons through the whisker-box plots, while in many further investigations in the following subsections, the mean values are used.

S7.2 Additional systematic factors: data processing-related factors and instrumental setup-related factors

Other factors potentially affecting the discrepancies between AMS-SP2 predicted hygroscopicity values and measured CCNC values are included in Supplementary Information, Notes S5: the chosen parameterization scheme of the CCNC SPAR curves' fittings, along with the adjustments, the chosen Köhler model, and the used minimum SSeff values. It was previously mentioned in the Results section that (Rose, D et al, 2008) found that the relative standard deviation of repeated measurements was less than 10% for effective supersaturation (Seff) >0.1% but exceeded 40% for Seff<0.1%. Meanwhile, in this current study, the experiments that were grouped as experiments conducted at SSeff =0.1% actually contained also experiments that were conducted a slightly lower than 0.1%. If less than 0.1% of the used SSeff has indeed possibly any influence in this current study, the interpretation of results could likely be better by firstly focusing the interpretation on the results of experiments conducted above 0.1% before including the results of experiments conducted at SSeff = below 0.1%.

S7.3 Detailed Explanation of Measurement Regime Factors' Effect on Inter-Method Discrepancies

S7.3.1. Surface Active Compounds

Surface-active compounds can modify hygroscopic behavior differently under either subsaturated or supersaturated conditions, due to the competing influences of surface tension effects, bulk–surface partitioning, and solution non-ideality, while bulk–surface partitioning of surfactants within particles itself depends on variables such as RH, solute mass ratio, and initial particle diameter. (Wokosin, K. A., et al, 2022). Furthermore, different surface-active compounds can even affect hygroscopicity differently through different configurations or arrangement of the molecules at the air-water interface. (Wokosin, K. A., et al, 2022). Some studies showed insensitivities of HTDMA kappa on surface active compounds (Müller A, et al, 2017). Some others, however, showed even negative impacts of surface-active compounds on the HTDMA subsaturated conditions (Zhang C et al, 2021). It could be that the surfactants form a hydrophobic organic layer at the surface that prevents water attraction, resulting in only limited water molecules being attracted to the particles. (Ruehl & Wilson, 2014). Meanwhile,

surface active compounds can increase the particles' activation to form cloud droplets due to the surface tension reduction, thus lowering the activation barrier near or after the activation point as previously mentioned. (Whitehead JD, et al., 2014; Gray B, et al., 2017; Müller A, et al., 2017; Zhang C, et al., 2023; Kawana K, et al., 2016).

Such differences may contribute to the generally higher κ values derived from CCNC measurements relative to those from HTDMA measurements or from AMS-SP2 based predictions in this current study. As can be understood from the κ-Kohler theory equation, especially in the form introduced in subsection 2.6 (Rose, D., et al 2008), reduction in surface tension can directly contribute to the increase wet droplet diameter under the same amount of humidity and same hygroscopicity parameter κ, specifically through its Kelvin Curvature effect term. Meanwhile, decrease in solute concentration affecting the Raoult's Law effect term should be indirectly captured in the κ values. If the accurate surfactant containing droplets' surface tension is present instead of pure water surface tension, then the competing reduced solute concentration effect of the surface-active compound presence should lead to reduced κ values. In the κ derivation calculation from either HTDMA or CCNc measurements conducted in this current study, no adjustment was done to either the Kelvin term or Raoult term regarding the possible presence of surface-active compounds in the particles. There was no adjustment on the input surface tension parameter value replacing the pure water surface tension value. Therefore, the dominating surface tension reduction effect of the surfactant presence during CCNc measurements can appear in higher values of the derived κ.

In a chemical composition based κ values prediction like the one done in this study, all the ideal assumptions were used – no adjustment on the surface tension either. Therefore, the predicted κ values show almost similar pattern with CCNC derived κ values due to highly significant OC:BC ratio differences, yet with lower values. Varied magnitude of the discrepancy between CCN-derived κ values and predicted κ values across the different experiment types reflects the variability of the total amount and strength of the surface-active compounds across the different experiment types.

S7.3.2. Particle Phase State and Morphology

Solid, semisolid, or viscous states can affect the water uptake of aerosol particles, whether under subsaturated or supersaturated conditions, whereas the basic Kohler theory, along with the ZSR mixing ratio, assumes a liquid-phase particle. A semi-solid state of particles in an organic-rich phase was reported to cause water uptake kinetic limitation (Mikhailov, E. F., et al., 2015). An article mentioned that smoke POA particles generated from the burning of peat were likely (semi)solid, with reduced viscosity driven by hygroscopic growth during the aging within the simulated chamber with higher RH, i.e., RH=65% compared to RH=15%, leading to increased oxygenation of the POA reflecting increased oxidation of the particles (Chen, J., et al 2022). Meanwhile, the RH values in our study are about 45-55% - a bit lower than the values in (Chen, J., et al 2022). Therefore, this may explain the lower values of both the calculated O:C ratio and the hygroscopicity of smoke particles from peat burning in the current study.

In addition, different morphologies, such as the presence of liquid-liquid phase separation instead of a homogenous well-mixed liquid phase as assumed in the Kohler theory, just like the partitions of surface-active compounds to the particle surface, can affect the hygroscopicity of the particles, particularly under supersaturated conditions. This was observed in a study that

generated and observed three ternary complex mixed aerosols, each containing different amino acids with similar O:C ratios yet different solubility (Ferdousi-Rokib, N., et al. 2025)

S7.3.3. Instrumental and kinetic related effect: organic gases co-condensation effect

A process specific to certain measurement may also contribute to differences between HTDMA- and CCNC-derived κ values. One such process is the co-condensation of semi-volatile organic compounds during measurement. HTDMA measurements are typically conducted under near-equilibrium conditions with relatively long residence times, allowing gas-phase species to repartition to the particle phase during humidification. This can enhance particle growth and increase the apparent hygroscopicity. In contrast, CCNC measurements involve shorter residence times and temperature gradients within the activation column, limiting the extent of gas–particle partitioning during the measurement. As a result, co-condensation effects may be more pronounced in HTDMA than in CCNC, introducing an additional source of divergence that is not directly related to the subsaturated versus supersaturated regime. However, this effect is expected to be secondary compared to the dominant influences of thermodynamic regime and surface activity, and it was not explicitly quantified in the present study.

Co-condensation between water vapour and organic gases can increase the apparent hygroscopicity parameter (κ) derived under subsaturated conditions and under supersaturated conditions Wang et al (2025). In other words, the co-condensation effect of semi-volatiles can enhance both particle growth and cloud droplet activation, as stated in Sapkal, MG et al (2025). Many studies leading to that finding were originally motivated by the observed increase in either cloud droplet number concentration (CDND) (Heikkinen L et al., 2024) or CCN number concentration.(Wang et al, 2025; Topping et al., 2013) associated with the organic vapours' presence (Topping et al., 2013; Juranyi Z et al, 2009), within especially modelling studies mimicking realistic atmospheric conditions. As stated by one of the modelling studies (Topping et al., 2013), condensation of semi-volatile organic vapours onto particles can promote additional condensational growth through both the added soluble mass of the droplets and the facilitated additional water uptake. The co-condensing vapor could be organic, inorganic, or a mixture of organic and inorganic gases. (Wang et al., 2025; Topping et al., 2013).

Hu et al. (2018) conducted a study observing the co-condensation effect through the HTDMA measurements under subsaturated conditions, motivated by those CCN activation and cloud droplet formation-related effects. The study showed that particle growth factors measured in the presence of both water vapour and condensable organic gases were higher than those measured in the absence of condensable organic vapour. The observed growth enhancement in HTDMA reflects both increased water uptake and additional particle growth driven by the organic vapour condensation itself. These processes are physically consistent with and mechanistically support the enhanced CCN activation and increased cloud droplet formation observed under supersaturated conditions.

On the other hand, results from most conventional streamwise CCN counters (CCNCs) instruments – like the one used in the current study- were claimed as not demonstrating the co-condensation effect (Sapkal MG, et al 2025). This was due to heat applied to the particles as they transit through the CCNC column of conventional CCNCs, which inadvertently led to a missed co-condensation effect, resulting in an underestimated CCN concentration in the real atmosphere; in addition to the limitation in achieving SS below 0.13% required for studying large hydrophilic particles. (Sapkal MG, et al 2025). This concerning issue was previously

mentioned in Hu et al. (2018), that suppressed saturation ratio of the organic components caused by heating within instruments, leading to raised saturation vapour pressure, thus decreased mixing ratio of the organic components, accompanied by too short residence times within the instruments can cause insensitivities to co-condensation of organic components at ambient concentrations.

A study examined the co-condensation effect in both HTDMA-CCNC instruments by using a charcoal diffusion denuder to remove organic gases prior to CCNc and HTDMA measurements. (Ravichandran et al., 2026). The results showed that denuding reduced the HTDMA-CCNC **κ** discrepancy, in contrast to studies without a denuding process reporting significantly higher CCNC-derived **κ** values than the corresponding HTDMA **κ** values. These may not seem supporting interpretation of the previous paragraphs that organic gases increasing HTDMA k while not affecting CCNC k so removing the gas should reduce the HTDMA k but keep the CCNC k constant. However, it is important to note that the removal of the compounds, especially using a denuder, can lead to re-equilibration prior to the instrument measurements. Therefore, results from the study in (Ravichandran et al., 2026) further showed that denuder use can either increase or decrease CCNc-derived **κ**, depending on relative humidity and

In both HTDMA and CCNC measurements – like those in current studies, aerosol particles are first dried using a silica gel or Nafion drier to remove adsorbed water and reduce the air RH to approximately below 30-40% (Ravichandran et al., 2026; Hass-Mitchell, 2024) or even below 5% (Malek, K.A., et al 2024). Following this drying process, semi-volatile compounds can be evaporated or partitioned into the gas phase, yielding additional gas-phase compounds that can undergo co-condensation with water vapour, thereby enhancing the measured hygroscopicity.

Based on Topping et al. (2013), co-condensation impacts are expected to be stronger for particles with higher organic mass fractions and smaller hygroscopic cores. This initially looked consistent with the CCNC-derived κ values' patterns in the current study. First, higher CCNC-derived κ values were observed for Leaves and Peat, whose particles exhibit higher organic content and lower inorganic fractions. In contrast, flaming particles with lower CCNC-derived κ values contain the lowest organic fraction and are therefore reasonably expected to experience a weaker water–organic vapour co-condensation effect, which would limit the enhancement of CCN activation. However, two important things should be considered.

First, the above interpretation should be expected to be valid if the organic vapor amounts are at least comparable or similar among the different burning phases. Higher organic vapor released during biomass burning under smouldering-phase conditions relative to under flaming-phase conditions was observed in many studies. (Li, R., et al. 2024; Garg, P., et al. 2024; Stefenelli, G., et al., 2019). However, no matter how the organic content of the particle phase and the gas phase of the smoke from whichever burn phases is, the current study used a conventional CCNC that can limit the possibility of an organic co-condensation event during the measurement. Therefore, cause(s) of the observed burn-phase separation in the CCNC-derived κ values may not, at least not primarily if however, any, be the co-condensation effects.

Notes S8: Proposed unified four-set experimental framework for future work

Although this study has identified several potential drivers of discrepancies among κ values derived from CCNC measurements, HTDMA measurements, and composition-based predictions, further work is required to quantify these effects more systematically and rigorously, particularly for processes that were not explicitly isolated here. We therefore propose a unified experimental framework consisting of four complementary sets of experiments for each fuel type and burn condition.

In the first set, measurements should be conducted at fixed particle sizes across multiple selected diameters, including HTDMA, CCNC operated using supersaturation scans rather than size scans, and AMS–SP2 measurements. This should be accompanied by explicit quantification of externally mixed non-hygroscopic fractions using HTDMA growth-factor distributions, CCNC activation-fraction data, and SP2 measurements. Known fractions of externally mixed non-hygroscopic black carbon should then be excluded from the composition-based prediction, and the corresponding non-hygroscopic fraction should also be removed from HTDMA-derived κ before comparison across the three approaches. This framework would allow systematic isolation of discrepancies arising from (i) size-dependent hygroscopicity and particle-size representation and (ii) the presence of externally mixed non-hygroscopic particles. The second set of experiments should follow the same protocol but include the removal of organic gases before aerosol measurements to suppress possible co-condensation effects. This should be coupled with gas-phase chemical measurements before and after gas removal to quantify the extent of gas-phase contributions both immediately after removal and after several minutes of equilibration, when particle–gas partitioning is expected to become more uniform before the start of the experiment or photo-ageing treatment. Such an approach would enable direct assessment of the role of co-condensation in modifying both subsaturated growth and supersaturated activation behaviour.

The third and fourth sets of experiments should repeat the first and second experimental designs, respectively, but with full inclusion of black carbon in the analysis. This step is essential for reintroducing the complete particle population after isolating individual discrepancy factors, thereby enabling evaluation of how mixing state and BC-containing particles influence bulk hygroscopicity under more realistic conditions. By comparing results obtained under isolated and full-population conditions, it would be possible to quantify how individual factors propagate into bulk κ and to assess the extent to which simplified assumptions affect interpretation.

Once the possibility of organic- and water-vapour co-condensation is isolated or minimized, and discrepancies associated with particle-size representation and mixing state are reduced, it may become possible to derive a quantitative correction framework linking κ values obtained from different measurement approaches. Such a framework, developed within a unified experimental system, could enable more consistent translation among HTDMA-derived, CCNC-derived, and composition-derived κ values. This would support more appropriate application of hygroscopicity data, for example by using HTDMA-derived κ for subsaturated processes such as visibility degradation and CCNC-derived κ for cloud activation and aerosol–cloud interaction studies.

In each set of experiments, additional measurements should be included to examine discrepancy factors associated with different physicochemical processes under subsaturated and supersaturated measurement regimes. These include measurements of particle surface tension and, where possible, detection of surface-active compounds to assess their role in enhancing CCN activation. Measurements of particle morphology and phase state, for example

using microscopy-based techniques, would also be useful for directly evaluating the influence of particle shape, phase separation, and viscosity on water uptake. In addition, particle density measurements would be valuable if HTDMA-derived mass-weighted average κ values are calculated and compared alongside number-weighted values, in order to avoid potential bias arising from the assumption of uniform effective particle density when converting SMPS number size distributions to mass size distributions.

Section 2. Supplementary Tables

Table S1. HTDMA available and used data during each 1-hour time interval after lights one*

Experiment Type	Initial	1st Hour	2nd Hour	3rd Hour	4th Hour	5th Hour	6th Hour
Peat_21Sep	50 nm, 75 nm	75 nm, 110 nm, 165 nm, 265 nm	75 nm, 110 nm, 265 nm	75 nm, 110 nm, 265 nm	75 nm, 110 nm, 265 nm	75 nm, 110 nm, 265 nm	75 nm, 110 nm, 265 nm
Peat_28Sep	75 nm, 110 nm, 265 nm	75 nm, 110 nm, 265 nm	75 nm, 110 nm, 265 nm	75 nm, 110 nm, 265 nm	75 nm, 110 nm, 265 nm	75 nm, 110 nm, 265 nm	75 nm, 110 nm, 265 nm
Leaves_16Sep	75 nm, 110 nm, 265 nm	75 nm, 110 nm, 265 nm	75 nm, 110 nm, 265 nm	75 nm, 110 nm, 265 nm	75 nm, 110 nm, 265 nm	75 nm, 110 nm, 265 nm	265nm
Leaves_26Sep	75 nm, 110 nm, 265 nm	75 nm, 110 nm, 265 nm	75 nm, 110 nm, 265 nm	75 nm, 110 nm, 265 nm	75 nm, 110 nm, 265 nm	75 nm, 110 nm, 265 nm	75 nm, 110 nm, 265 nm
Leaves_27Sep	75 nm, 110 nm, 265 nm	75 nm, 110 nm, 265 nm	75 nm, 110 nm, 265 nm	75 nm, 110 nm, 265 nm	75 nm, 110 nm, 265 nm	75 nm, 110 nm, 265 nm	75 nm, 110 nm, 265 nm
Leaves_29Sep	75 nm, 110 nm, 265 nm	75 nm, 110 nm, 265 nm	75 nm, 110 nm, 265 nm	75 nm, 110 nm, 265 nm	75 nm, 110 nm, 265 nm	75 nm, 110 nm, 265 nm	
Smouldering_ Hardwood_ 20Apr	50 nm, 75 nm, 110 nm	50 nm, 75 nm, 110 nm	50 nm, 75 nm, 110 nm	50 nm, 75 nm, 110 nm, 165 nm	50 nm, 75 nm, 110 nm, 165 nm, 265 nm	50 nm, 75 nm, 110 nm, 165 nm, 265 nm	50 nm, 75 nm, 165 nm, 265 nm
Smouldering_ Hardwood_ 26Apr		50 nm, 75 nm, 110 nm	50 nm, 75 nm, 110 nm	50 nm, 75 nm, 110 nm, 165 nm	50 nm, 75 nm, 110 nm, 165 nm, 265 nm	50 nm, 75 nm, 110 nm, 165 nm, 265 nm	50 nm, 75 nm, 165 nm, 265 nm
Smouldering_ Hardwood_ 31Aug				75 nm, 110 nm, 265 nm	75 nm, 110 nm, 265 nm	75 nm, 110 nm, 265 nm	75 nm, 110 nm, 265 nm
Non_Photoageing _Smouldering_ Hardwood_ 19Apr	N/A		50 nm 75 nm 110 nm	50 nm 75 nm 110 nm	50 nm 75 nm 110 nm	50 nm 75 nm 110 nm	75 nm 110 nm
Smouldering_ Softwood_ 08Apr	50 nm, 75 nm, 110 nm	50 nm, 75 nm, 110 nm	50 nm, 75 nm, 110 nm	50 nm, 75 nm, 110 nm	50 nm, 75 nm, 110 nm	50 nm, 75 nm, 110 nm	50 nm, 75 nm, 110 nm
Smouldering_ Softwood_ 06Sep	50 nm, 75 nm, 110 nm, 165nm, 265nm	50 nm, 75 nm, 110 nm, 165nm, 265nm	50 nm, 75 nm, 110 nm, 165nm, 265nm	75 nm, 110 nm, 265nm	75 nm, 110 nm, 265nm	75 nm, 110 nm, 265nm	110 nm
Smouldering_ Softwood_ 15Sep				75 nm, 110 nm, 265nm	75 nm, 110 nm, 265nm	75 nm, 110 nm, 265nm	75 nm, 110 nm, 265nm
Non_Photoageing							

Smouldering Softwood_ 06Apr							
Flaming_ Hardwood_ 30Aug	50 nm, 75 nm, 110 nm, 165 nm, 265 nm	50 nm, 75 nm, 110 nm	50 nm, 75 nm, 110 nm	50 nm, 75 nm, 110 nm	50 nm, 75 nm, 110 nm	50 nm, 75 nm, 110 nm	50 nm, 75 nm, 110 nm
Flaming_ Hardwood_ 22Sep	75 nm, 110 nm, 165 nm	75 nm, 110 nm, 165 nm	75 nm, 110 nm, 165 nm	75 nm, 110 nm, 165 nm	75 nm, 110 nm, 165 nm	75 nm, 110 nm, 165 nm	75 nm, 110 nm, 165 nm
Non_Photoageing _Flaming_ Hardwood_ 22Apr							
Non_Photoageing _Flaming_ Hardwood_ 29Apr							
Flaming_ Softwood_ 07Apr	50 nm, 75 nm, 110 nm	50 nm, 75 nm, 110 nm	50 nm, 75 nm, 110 nm	50 nm, 75 nm, 110 nm, 165nm	50 nm, 75 nm, 110 nm, 165nm	50 nm, 75 nm, 110 nm, 165nm	50 nm, 75 nm, 110 nm, 165nm
Non_Photoageing _Flaming_ Softwood_ 11Apr							
Flaming_ Softwood_ 01Sep	75 nm, 165 nm, 265nm	75 nm, 110 nm, 165nm a265nm	75 nm, 110 nm, 265 nm	75 nm, 110 nm, 265 nm	75 nm, 110 nm, 265 nm	75 nm, 110 nm, 265 nm	75 nm, 110 nm, 265 nm

*The grey shaded rows were the unused data in the HTDMA measured versus predicted κ comparison due to unavailable SP2 data.

Table S2. CCNC available and used data during the whole experiment time period*

Experiment Type	SuperSaturation
Peat_14Sep	0.1%; 0.3%; 0.5%
Peat_21Sep	0.1%; 0.3%; 0.5%
Peat_28Sep	0.1%; 0.3%; 0.5%
Leaves_16Sep	0.1%; 0.3%; 0.5%
Leaves_26Sep	0.1%; 0.3%; 0.5%
Leaves_27Sep	0.1%; 0.3%; 0.5%
Leaves_29Sep	0.1%; 0.3%; 0.5%
Smouldering_Hardwood_20Apr	0.1%; 0.3%; 0.6%;0.8%;1%;
Smouldering_Softwood_08Apr	0.1%; 0.3%; 0.6%;0.8%;1%;
Smouldering_Softwood_14Apr	0.1%; 0.3%; 0.6%;0.8%;1%;
Smouldering_Softwood_06Sep	0.1%; 0.3%; 0.6%
Smouldering_Softwood_15Sep	0.3%; 0.6%
Non_Photoageing_ Smouldering_Softwood_06Apr	
Flaming_Hardwood_21Apr	0.1%; 0.3%; 0.6%;0.8%;1%
Flaming_Hardwood_28Apr	0.1%; 0.3%; 0.6%;0.8%;1%
Flaming_Hardwood_22Sep	0.1%; 0.3%; 0.6%

Non_Photoageing_ Flaming_Hardwood_29Apr	
Flaming_Softwood_07Apr	0.1%; 0.3%; 0.6%;0.8%;1%
Flaming_Softwood_13Apr	0.1%; 0.3%; 0.6%;0.8%;1%
Non_Photoageing_ Flaming_Softwood_11Apr	

* The grey shaded rows were the unused data in the CCNC measured versus predicted κ comparison due to unavailable SP2 data

Table S3. Available hourly averaged data used for HTDMA versus CCNC data set

Experiment Type	CCNC DATA (SS values)	HTDMA DATA
Peat_21Sep	0.1%;0.5%	Size number weighted
Peat_28Sep	0.1%; 0.3%; 0.5%	Size number weighted
Leaves_16Sep	0.1%; 0.3%; 0.5%	Size number weighted
Leaves_26Sep	1%; 0.3%; 0.5%	Size number weighted
Leaves_27Sep	0.1%; 0.3%; 0.5%	Size number weighted
Leaves_29Sep	.1%; 0.3%; 0.5%	Size number weighted
Smouldering_Hardwood_20Apr	0.1%; 0.3%; 0.6%;0.8%;1%;	Size number weighted
Smouldering_Softwood_08Apr	0.1%; 0.3%; 0.6%;0.8%;1%;	Size number weighted
Smouldering_Softwood_06Sep	0.1%; 0.3%; 0.6%	Size number weighted
Smouldering_Softwood_15Sep	0.3%; 0.6%	Size number weighted
Non_Photoageing_ Smouldering_Softwood_06Apr		
Flaming_Hardwood_22Sep	0.1%; 0.3%; 0.6%	Size number weighted
Non_Photoageing_ Flaming_Hardwood_29Apr		
Flaming_Softwood_07Apr	0.1%; 0.3%; 0.6%;0.8%;1%	Size number weighted
Non_Photoageing_ Flaming_Softwood_11Apr		

Table S4. Various Approaches for Using Chemical Composition Based Hygroscopicity Prediction

Literature	Volume Fraction or Mass Fraction	BC Inclusion	Inorganic Determination or Assumption	Organic K	Inorg K	BC K	Org density	Inorg density	BC density
Gysel et al 2007	Volume Fraction Reilly and Wood (1969)	No	Single ion pairing algorithm	0.1	(NH4)2SO4: 0.47 NH4HSO4: 0.56 NH4NO3: 0.58 H2SO4: 0.91	N/A	1400	(NH4)2SO4: 1769 NH4HSO4: 1720 NH4NO3: 1780 H2SO4: 1830	N/A

Chang et al 2010	Volume fraction	No	Group containing ammonium, nitrate, and sulphate behaves like ammonium sulphate	Calculated Based on O/C vs Hygroscopicity,	0.59	N/A			
Kim N et : a) **Modified** Gysel2007-Chang2010	Volume fraction	No	Single ion pairing algorithm	Calculated Based on O/C vs Hygroscopicity: K org = 0.29 x O/C	(NH4)2SO4: 0.47 NH4HSO4: 0.56 NH4NO3: 0.58 H2SO4: 0.91	N/A	1400	(NH4)2SO4: 1769 NH4HSO4: 1720 NH4NO3: 1780 H2SO4: 1830	N/A
Kim N et al 2017: b) **Optimised** Gysel2007-Chang2010 Remove data with high NH4NO3 fraction (>0.2)	Volume fraction	Yes; From MAAP PM 2.5 measurment with assumption dominant BC mass in submicron particles	Single ion pairing algorithm	1st version: Calculated Based on O/C vs Hygroscopicity: K org = 0.29 x O/C 2nd version: Calculated From K HTDMA subtracted by the sum of the listed inorganic κ x volume fraction, ##### Just for check/comparison: Recalculated O/C vs hygroscopicity K org = 0.1 x O/C with low correlation	(NH4)2SO4: 0.47 NH4HSO4: 0.56 NH4NO3: 0.58 H2SO4: 0.91	0	1400	(NH4)2SO4: 1769 NH4HSO4: 1720 NH4NO3: 1780 H2SO4: 1830	1700
Fan X et al, 2020	Volume Fraction	Yes	The inorganic components mainly consisted of (NH4)2SO4 and NH4NO3;	Calculated Based on f44 vs Hygroscopicity	K values of (NH4)2SO4 = 0.48; K values of NH4NO3 = 0.58.	0	1.2	(NH4)2SO4 = 1.77gcm3 NH4NO3 = 1.72gcm3	N/A

Healy et al 2014	Volume Fraction	Yes	Inorganic mass fraction = ammonium mass fraction, sulphate mass fraction, nitrate mass fraction; Inorganic volume fraction = Inorganic mass fraction/Inorganic density	Calculated Based on O/C vs Hygroscopicity, Result: Organic GF= 1.2	GF=1.66	GF=1	1.44	1.77	2
Che, HC et al. 2017	Mass Fraction, Justification: first-order approximations): **"Similar density of each component to the overall particle density."**	No	Not explicitly stated	0.1	0.6	N/A	N/A	N/A	N/A
Gunthe et al 2009	Mass Fraction	No	All inorganic species including SO42-, NO3-, and NH4+ are assumed as sulphate	0.1	0.6	N/A	N/A	N/A	N/A
Pohkler, ML et al. 2023	Mass Fraction; Justification:	No	Inorganic mass = SO4 mass + NO3 mass + NH4 mass + Cl mass	To be revealed through Measured K vs component fraction	To be revealed through Measured K vs component fraction	N/A	N/A	N/A	N/A
Li, C et al 2016	Mass	Yes, But not only into the total mass -> included to the Organic too	Using offline filter chemical composition measurement	To be revealed through Measured K vs component fraction	To be revealed through Measured K vs component fraction	N/A	N/A	N/A	N/A

Table S5. Predicted to Measured HTDMA Hourly Mean κ Ratio; Note: prediction input: κ_{Org}=0.1, κInorg=0.6, κBC=0;

Experiment Type	Predicted to Measured HTDMA κ Ratio											
	NumberWeighted		Dp =50 nm		Dp =75nm		Dp =110nm		Dp =165nm		Dp =265nm	
	Mean	Std	Mean	Std	Mean	Std	Mean	Std	Mean	Std	Mean	Std
Peat	8.0486	21.9226			7.94	12.63	-26.66	131.76	N/A	N/A	19.32	71.33
Leaves	2.5681	0.8874	-	-	1.48	0.72	1.70	0.56	-	-	3.49	0.42
Flaming Hardwood	5.6363	3.2590			1.48	0.73	8.65	9.48			N/A	N/A
Smouldering Hardwood	4.0439	8.1249			8.30	15.31	0.95	0.21				
Flaming Softwood	0.6871	0.3155			0.49	0.21	0.91*	0.47				
Smouldering Softwood	1.6405	0.3844			1.59	1.30	1.78	1.07				

*Ignore data with measured κ = 0

Table S6. Predicted to Measured CCNC Hourly Mean κ Ratio. Note: prediction input: kOrg=0.1, kInorg=0.6, kBC=0;

Experiment Type	Predicted to Measured CCNC K Ratio											
	All SS		SS=0.1%		SS=0.3%		SS=0.5-0.6%		SS=0.8%		SS=1%	
	Mean	Std	Mean	Std	Mean	Std	Mean	Std	Mean	Std	Mean	Std
Peat	0.6409	0.4374	0.5024	0.2420	0.6104	0.3815	0.7755	0.5673	N/R	N.R	N/R	N/R
Leaves	1.1189	0.9728	0.4073	0.1083	0.5598	0.2470	1.9870	0.9492	N/R	N/R	N/R	N/R
Flaming Hardwood	0.7633	1.1737	0.6174	0.4329	0.7955	1.0481	0.7858	1.9043	0.6667	0.4511	0.9471	1.0860
Smouldering Hardwood	1.0071	0.4599	0.7124	0.1437	0.8996	0.0452	0.7876	0.3404	1.1442	0.2367	1.4647	0.7094
Flaming Softwood	0.9022	0.4048	1.0268	0.4794	1.0668	0.3569	0.9532	0.4741	0.8151	0.3715	0.7419	0.3334
Smouldering Softwood	1.2721	1.8002	0.9167	0.4487	1.3778	0.5331	1.0630	0.5919	2.0992	4.1989	1.0417	0.4477

*N/R: Not Recorded

Table S7. Organic and inorganic κ reveal with all data points

Experiment Type	Inorganic κ	Mean Organic κ	R^2
Peat	1.1038	-0.0121	0.5693
Leaves	0.4472	0.0310	0.0817
Flaming Hardwood	0.6372	-0.0806	0.2654
Smouldering Hardwood	0.0040	0.0753	0.00015
Flaming Softwood	1.1678	0.1293	0.6160
Smouldering Softwood	0.3228	0.0702	0.1135

Table S8. Organic and inorganic κ revealed, with the box-and-whisker plot-detected outliers of the peat experiment, flaming hardwood experiment, and smouldering hardwood removed

Experiment Type	Inorganic κ	Mean Organic κ	R^2
Peat	0.6256	-0.0014	0.2784
Leaves	0.4472	0.0310	0.0817
Flaming Hardwood	0.0535	0.0420	0.2654
Smouldering Hardwood	-0.0822	0.0876	0.3849
Flaming Softwood	0.8575	0.2000	0.6610

Smouldering Softwood	0.3228	0.0702	0.1135

Table S9. Factors affecting discrepancy between HTDMA number-weighted measured κ values and chemical composition-based predicted κ values, as mentioned in the previous subsection include

No	Factors	Validation	Further required validation	Type of the factors
1	Representation of the selected tested particle size(s) and the presence of size-dependent hygroscopicity.	slightly validated, through: 1. Comparison between the tested number-weighted mean HTDMA κ values and the mean SMPS particle size 2. κ values comparison between different sizes to detect the presence of size-dependent hygroscopicity 3. Additional comparison with mass-weighted mean HTDMA κ	Conduct experiments with more consistent and more complete number of the tested sizes and time points to match either the number mean size (to be compared with CCNc measured k or volume fraction-based AMS-SP2 predicted κ), or Mass mean size(to be compared with mass fraction-based AMS-SP2 predicted κ)	Combined (systematic and physical/chemical factor, i.e., presence of size-dependent hygroscopicity that could be varied across different experiment type)
2	More varied and higher organic κ values	Slightly validated through: 1. Comparison with the pattern of the calculated O:C ratio and equation based κ_{org} pattern 2. Comparison between the initial predicted to measured ratio and the new initial predicted to measured ratio using new κ_{org} values obtained from the adjusment	1) Remove or Eliminate contribution from other factors first, then 2.a) re-examine or recompare the HTDMA measured κ 2.b) did more accurate organic κ determination then re-calculate and recompare the obtained predicted κ	Chemical-related factors

		from 0.1 according to the AMS-O:C ratio values variability pattern accros the 6 experiment types		
3	Presence of surface-active substances in the particle phase	Assumed or not validated	Conduct morphology check and chemcial analysis of the surfactant detection	Chemical-related factors
4	Use of mass fraction instead of volume fraction in the prediction	Assumed or not validated	Possibly dedicated experiments to test this factor and compared each other between mass fraction and volume fraction	Systematic/combines
5	Particles' phase state	Assumed or not validated	Morphology check of the particles and comparison with the k values	Physical-related factors

Table S10. Factors affecting the discrepancy between CCNc measured κ values and chemical composition-based predicted κ values

No	Factors	Validation	Further required validation	Type of the factors
1	Systematic size representation difference and presence of size-dependent hygroscopicity	Assumed or not validated	1. Comparison of the D50 values and the mass-weighted mean particle size 2. Size-dependent CCNc measured κ values 3. Size resolved chemical composition	Systematic / combination
2	Systematic data processing related factor in dealing with the presence of external mixture and/or size-dependent hygroscopicity	Partly validated (the presence of an external mixture)	1. Prove the presence of an external mixture 2. Try to differentiate between pure non hygroscopic BC and coated BC then compare AMS-SP2 predicted κ values that remove the pure BC	Systematic

			contribution with CCNC κ 3. Make a number weighted conversion of the current CCNc measured values to more represent the whole population by using the |1-max AF| data representing amount of the non hygroscopic fraction.	
3	Other Systematic factors: data processing-related factors and instrumental setup-related factors	Assumed or not validated	Ensure to use SSeff more than 0.1%	Systematic
4	Presence of surface-active substance in the particles	Assumed or not validated	Chemical analysis of the surface-active substance in the particles	Chemical-Physical-related factors

Table S11. Comparison of predicted-to-CCNc measured κ values ratio that resulting from prediction that added the Black Carbon as part of the total particle mass (old/current ratio) and those that did not (new ratio)

Experiment	Old ratio	New ratio	|ratio_old−1|	|ratio_new−1|	% Old error	% New error	More accurate
Peat	0.6419	0.6419	0.3581	0.3581	−35.81%	−35.81%	-
Leaves	1.1159	1.1387	0.1159	0.1387	+11.59%	+13.87%	Old κ
Hardwood (Flaming)	0.7683	2.6493	0.2317	1.6493	−23.17%	+164.93%	Old κ
Hardwood (Smouldering)	1.0491	1.0928	0.0491	0.0928	+4.91%	+9.28%	Old κ
Softwood (Flaming)	0.9002	3.3341	0.0998	2.3341	−9.98%	+233.41%	Old κ
Softwood (Smouldering)	1.2721	1.4134	0.2721	0.4134	+27.21%	+41.34%	Old κ

Table S12. Improvement percentage, i.e. the lost error contribution to the initial total error of the prediction relative to the HTDMA mean κ values resulted from choosing different particle size between 110 nm and 75 nm that has closer HTDMA mean κ value to the corresponding mean predicted κ value; **Notes**: Each value in the table is averaged values across the time points data in the corresponding experiment date, therefore reflecting also the mean data across different stage of aging from freshly emitted to 5-6 hours of aging.

Experiment Name (Type and Date)	Mean Predicted κ	HTDMA Mean κ at Particle Size of 110 nm	HTDMA Mean κ at Particle Size of 75 nm	% Improvement (Error contribution to the initial total error, %)
F_HW_20220922	0.057	0.024	0.041	66.43
NP_F_HW_20220422	0.058	0.022	0.043	67.84
S_HW_20220420	0.141	0.071	0.076	21.02
S_HW_20220426	0.131	0.003	0.015	67.92
S_HW_20220831	0.126	0.074	0.082	23.63
NP_S_HW_20220419	0.195	0.049	0.057	20.56
F_SW_20220407	0.082	0.070	0.124	43.60
F_SW_20220901	0.043	0.163	0.142	23.22
NP_F_SW_20220411	0.045	0.035	0.070	41.27
S_SW_20220408	0.142	0.081	0.093	62.93
S_SW_20220906	0.114	0.075	0.119	83.16
Peat_20220921	0.109	0.014	0.031	85.35
Peat_20220928	0.116	0.038	0.058	46.14
Leaves_20220926	0.130	0.048	0.047	14.58
Leaves_20220927	0.125	0.088	0.104	44.86
Leaves_20220929	0.129	0.094	0.150	61.44

Table S13. Improvement percentage, i.e. the lost error contribution to the initial total error of the prediction relative to the HTDMA mean κ values resulted from changing the weighted approaches (number-weighted versus mass-weighted); **Notes**: Each value in the table is averaged values across the time points data in the corresponding experiment date, therefore reflecting also the mean data across different stage of aging from freshly emitted to 5-6 hours of aging.

Experiment Name (Type and Date)	Mean Predicted κ	Number Weighted Mean HTDMA κ	Mass Weighted Mean HTDMA κ	% Improvement (Error contribution to the initial total error, %)
F_HW_20220922	0.057	0.019	0.013	-85.72
NP_F_HW_20220422	0.058	0.112	0.130	-67.58
S_HW_20220420	0.141	0.071	0.069	-6.88
S_HW_20220426	0.131	0.003	0.001	-483.58
S_HW_20220831	0.126	0.075	0.057	-68.48
NP_S_HW_20220419	0.193	0.055	0.052	**-8.05**
F_SW_20220407	0.082	0.114	0.069	**79.37**
F_SW_20220901	0.040	0.093	0.055	**58.30**
NP_F_SW_20220411	0.045	0.030	0.048	**79.71**
S_SW_20220408	0.142	0.087	0.083	-108.13
S_SW_20220906	0.114	0.112	0.055	**29.46**
Peat_20220921	0.109	0.012	0.004	-40.66

Peat_20220928	0.116	0.027	0.014	-58.83
Leaves_20220926	0.130	0.044	0.042	-15.75
Leaves_20220927	0.125	0.070	0.040	-141.11
Leaves_20220929	0.129	0.060	0.040	-63.89

Table S14. Improvement percentage, i.e. the lost error contribution to the initial total error of the prediction relative to the HTDMA mean κ values resulted from changing the initially used assumed organic κ value of 0.1 so that it become experiment types' mean O:C ratio value dependent; **Notes**: Each value in the table is averaged values across the time points data in the corresponding experiment date, therefore reflecting also the mean data across different stage of aging from freshly emitted to 5-6 hours of aging. *Note that CCNC prediction accuracy error changes and change percentages were averaged across both time points and supersaturation levels.

Experiment Name (Type and Date)	Predicted κ - Base	Predicted κ - Revised	CCNC	CCNC improvement	HTDMA κ	HTDMA improvement
F_HW_20220421	0.065	0.076	0.099	-12.67*		
F_HW_20220428	0.061	0.061	0.132	**0.004**		
F_HW_20220922	0.057	0.0570	0.313	**2.468***	0.019	-17.07
NP_F_HW_20220422	0.058	0.0569			0.112	-923.95
S_HW_20220420	0.141	0.151	0.163	**1.956**	0.071	-15.79
S_HW_20220426	0.131	0.122			0.003	**4.64**
S_HW_20220831	0.126	0.164			0.075	-73.70
NP_S_HW_20220419	0.195	0.129			0.054	**46.95**
F_SW_20220407	0.082	0.089	0.159	**1.633**	0.114	**15.91**
F_SW_20220413	0.063	0.073	0.058	-45.981		
F_SW_20220901	0.040	0.047			0.093	**14.98**
NP_F_SW_20220411	0.045	0.049	0.073	**3.481**	0.030	-35.41
S_SW_20220408	0.142	0.152	0.120	-0.080	0.087	**40.84**
S_SW_20220414	0.127	0.136	0.110	-15.611		
S_SW_20220906	0.114	0.132	0.335	**9.233**	0.112	-0.46
Peat_20220914	0.115	0.088	0.117	**22.986***		
Peat_20220921	0.111	0.080	0.269	-28.043	0.012	**32.66**
Peat_20220928	0.116	0.090	0.275	-19.690	0.027	**29.92**
Leaves_20220926	0.130	0.138	0.217	-0.075	0.044	-10.23
Leaves_20220927	0.125	0.098	0.192	**0.047***	0.070	-1.66
Leaves_20220929	0.129	0.091	0.210	**0.147***	0.060	**9.82**

Section 3. Supplementary Figures

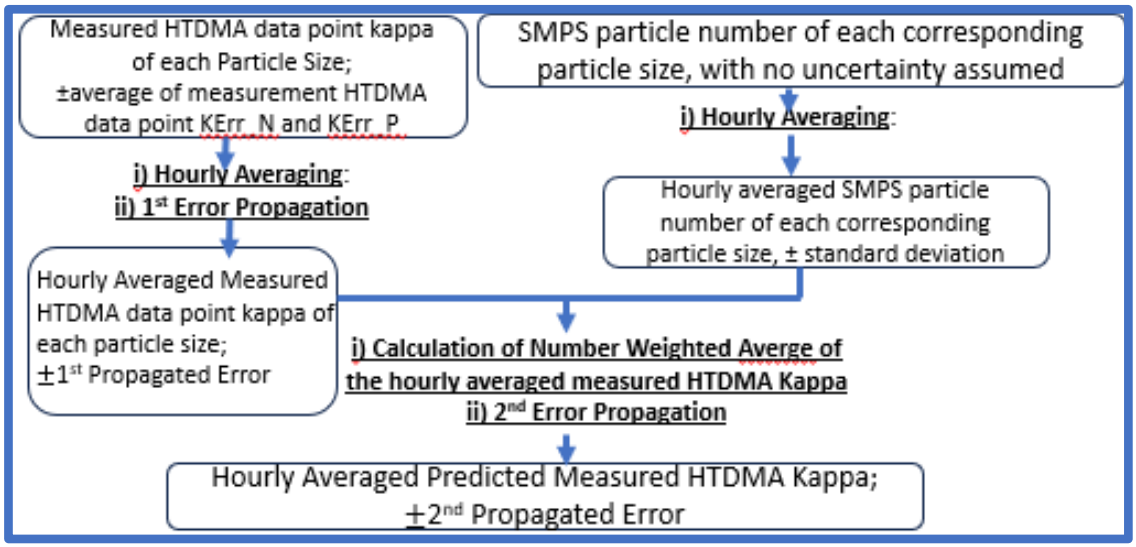

a)

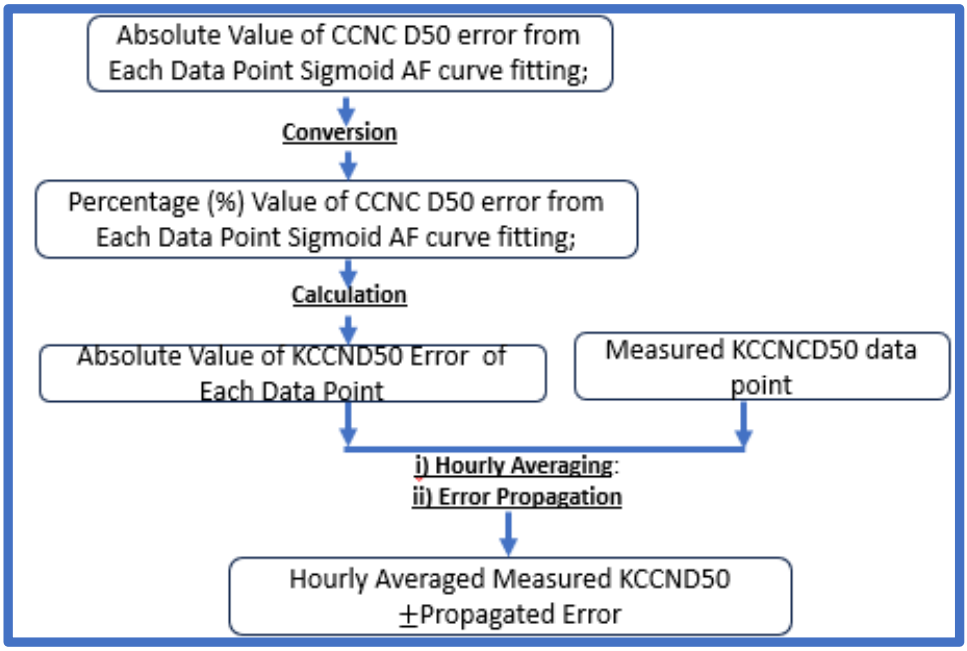

b)

Figure S1. HTDMA **a**) and CCNC **b**) Averaging and Corresponding Error Propagations FlowChart

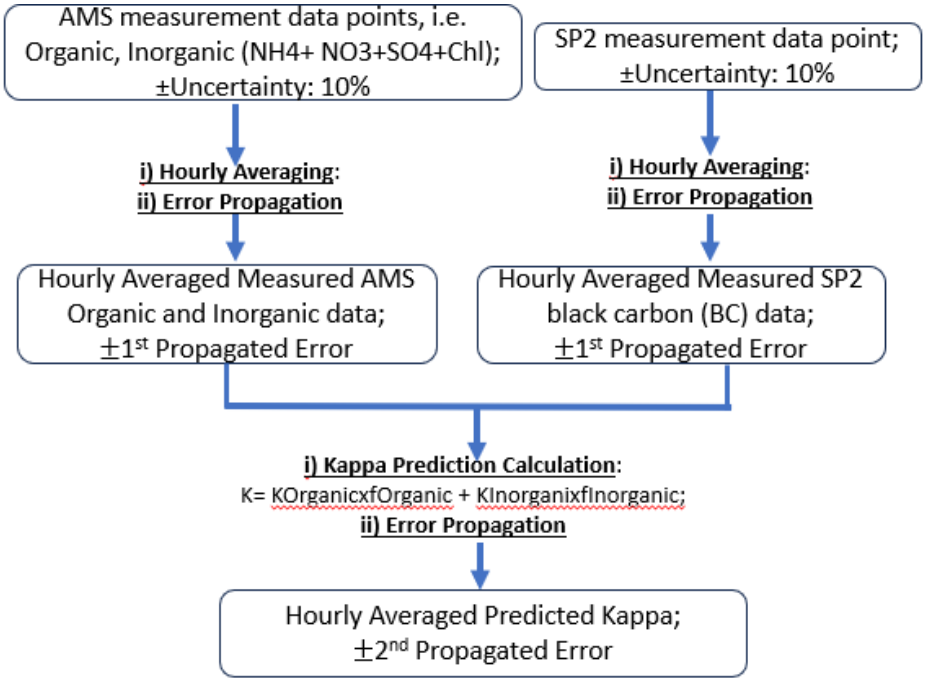

Figure S2. AMS-SP2 chemical composition based predicted kappa values Averaging and Corresponding Error Propagations FlowChart

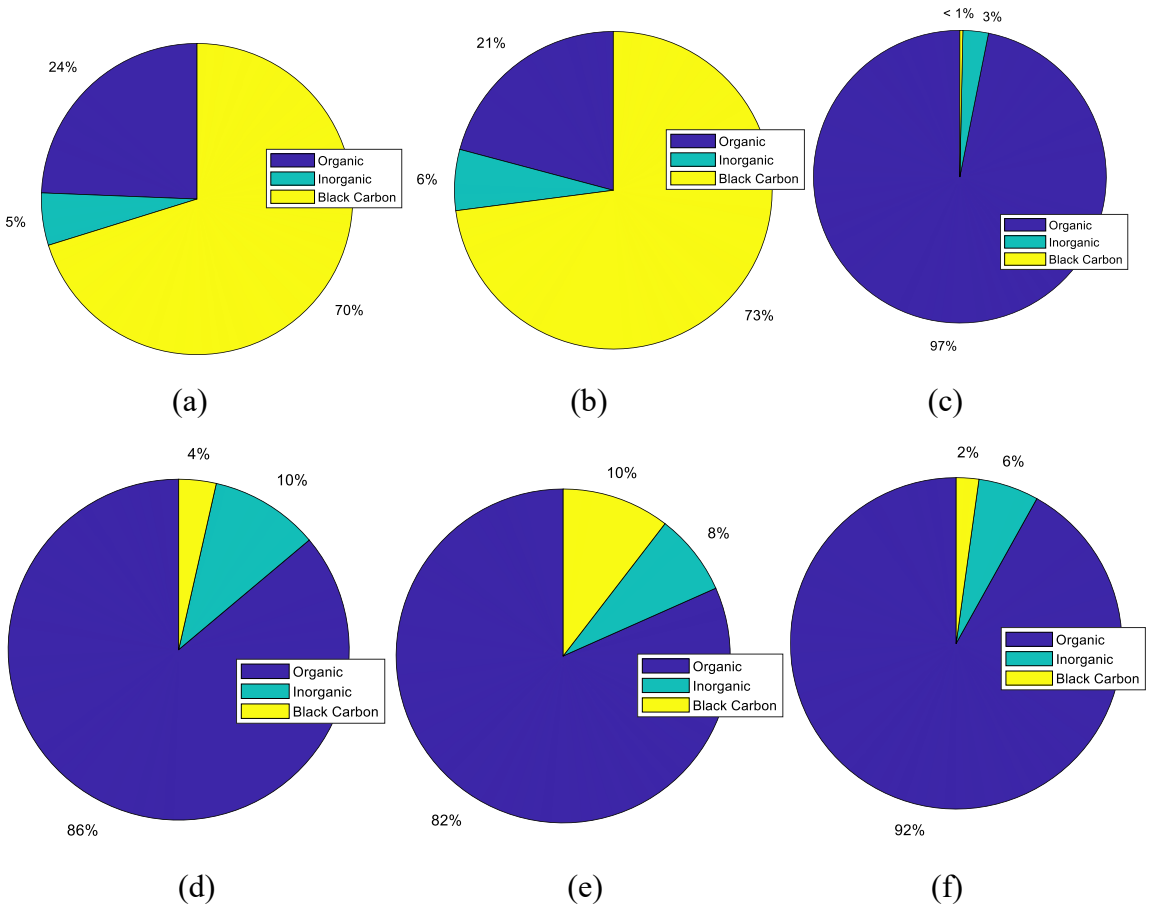

Figure S3. Averaged Chemical Composition Pie Charts F_HW (a), F_SW (b), Peat (c), S_HW (d), S_SW (e), Leaves (f)

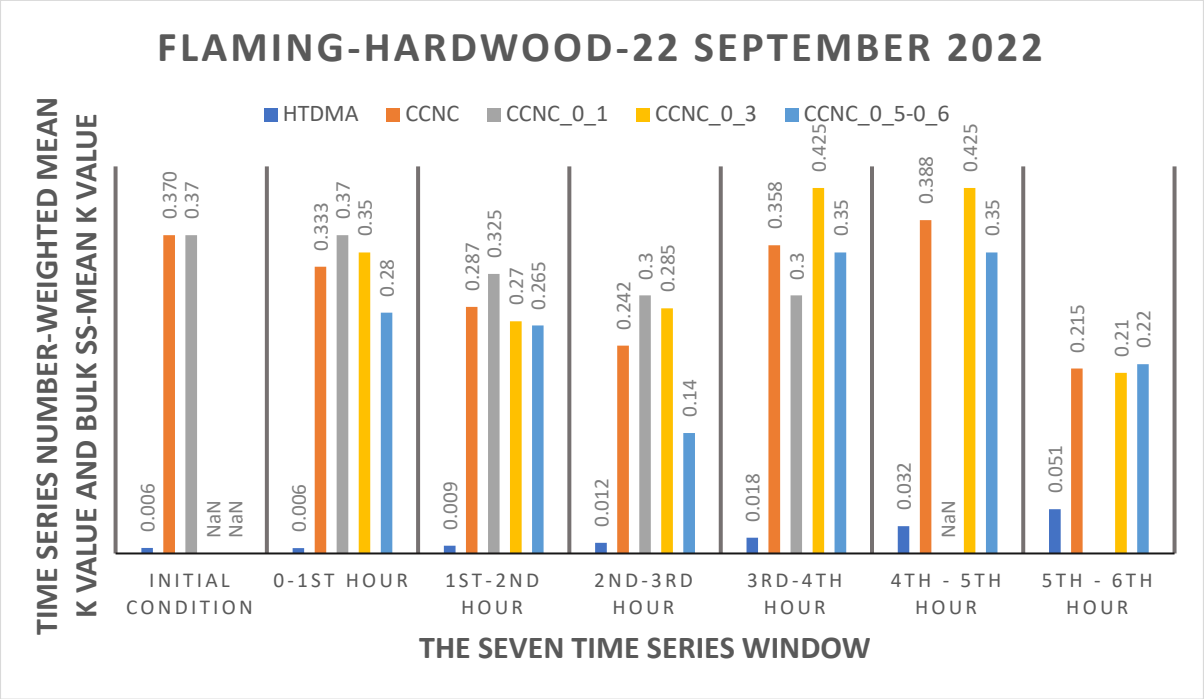

(a)

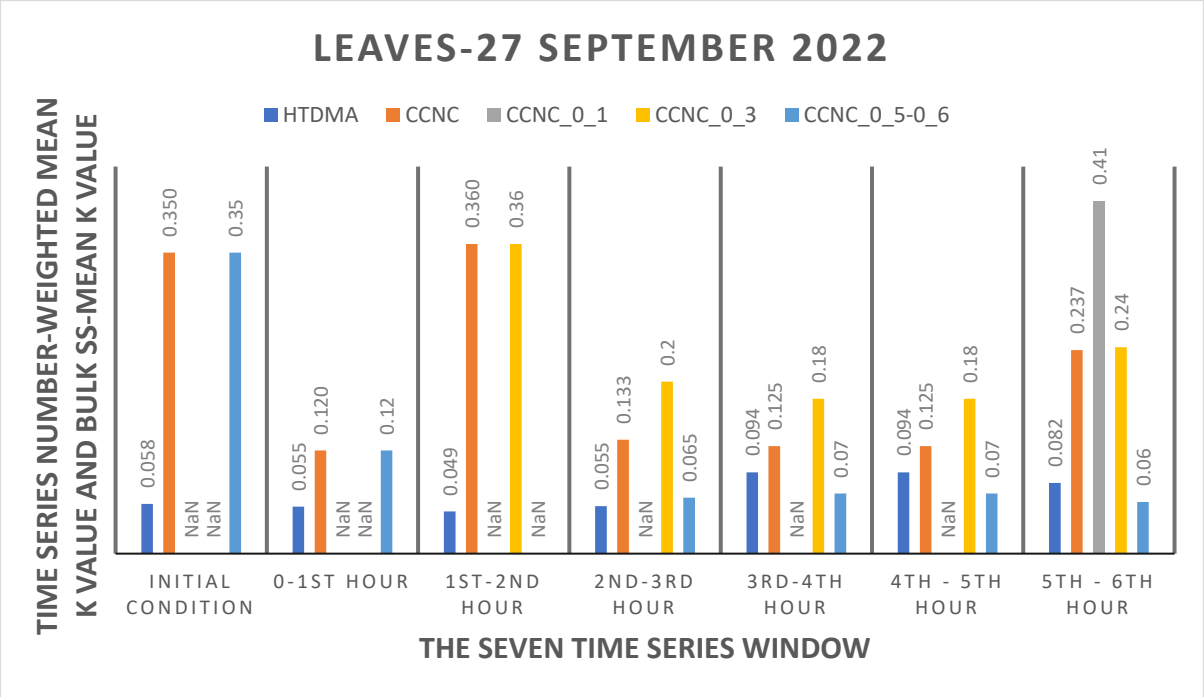

(b)

Figure S4. Time variability of the HTDMA number-weighted mean kappa and CCNC mean kappa (all SS-averaged, SS_0.1%, SS_0.3%, SS_0.5-0.6%) of the Flaming-Hardwood Experiment- 22 September 2022, and Leaves Experiment-27 September 2022

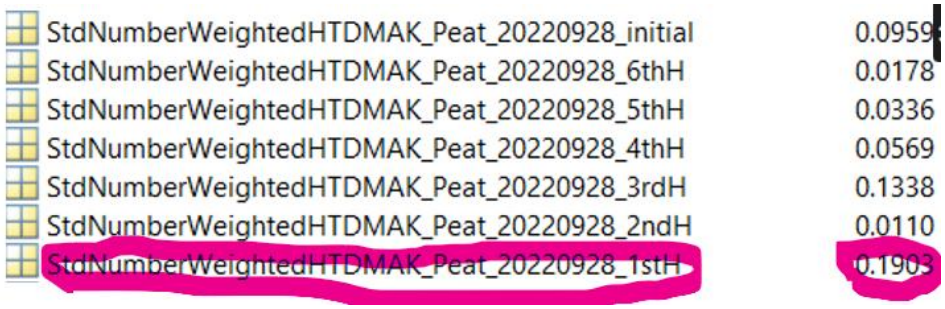

(a)

HTDMA_PL_Peat_28Sep_1stH_110nm | HTDMA_PL_Peat_28Sep_1stH_265nm

3x13 table

	1 Time	2 K	3 D	4 Kmin	5 Kmax	6 GF	7 GFsdev	8 RH_corrected	9 kappaErrN	10 kappaErrP	11 AvgKError	12 TAES	13 TALON
1	28-Sep-2022 10:35...	0.0172	110	-0.0541	0.0958	1.0122	0.0523	69.6004	0.0172	0.0786	0.0479	00:49:02	00:05:02
2	28-Sep-2022 11:01...	0.0437	110	-0.0391	0.1363	1.0318	0.0619	70.6644	0.0437	0.0926	0.0682	01:15:23	00:31:23
3	28-Sep-2022 11:27...	0.0175	110	-0.0481	0.0898	1.0137	0.0534	71.9060	0.0175	0.0724	0.0449	01:41:44	00:57:44

(b)

Variables - HTDMA_PL_Peat_28Sep_1stH_265nm

HTDMA_PL_Peat_28Sep_1stH_110nm | HTDMA_PL_Peat_28Sep_1stH_165nm | HTDMA_PL_Peat_28Sep_1stH_265nm

2x13 table

	1 Time	2 K	3 D	4 Kmin	5 Kmax	6 GF	7 GFsdev	8 RH_corrected	9 kappaErrN	10 kappaErrP	11 AvgKError	12 TAES	13 TALON
1	28-Sep-2022 10:43...	-0.0176	265	-0.1160	0.0924	0.9904	0.0572	62.3369	0.1101	0.1101	0.1101	00:57:49	00:13:49
2	28-Sep-2022 11:10...	0.0057	265	-0.0986	0.1234	1.0032	0.0621	63.3490	0.1177	0.1177	0.1177	01:24:10	00:40:10

(C)

HTDMA_PL_Peat_28Sep_1stH_110nm | HTDMA_PL_Peat_28Sep_1stH_265nm | HTDMA_PL_Peat_28Sep_2ndH_110nm | HTDMA_PL_Peat_28Sep_2ndH_165nm | HTDMA_PL_Peat_28Sep_2ndH_265nm

3x13 table

	1 Time	2 K	3 D	4 Kmin	5 Kmax	6 GF	7 GFsdev	8 RH_corrected	9 kappaErrN	10 kappaErrP	11 AvgKError	12 TAES	13 TALON	14	15
1	28-Sep-2022 11:36...	0.0275	265	-0.0629	0.1280	1.0161	0.0549	64.6127	0.1005	0.1005	0.1005	01:50:31	01:06:31		
2	28-Sep-2022 12:02...	0.0341	265	-0.0548	0.1333	1.0214	0.0579	66.3906	0.0992	0.0992	0.0992	02:16:53	01:32:53		
3	28-Sep-2022 12:29...	0.0189	265	-0.0562	0.1021	1.0128	0.0527	67.7850	0.0832	0.0832	0.0832	02:43:14	01:59:14		

(d)

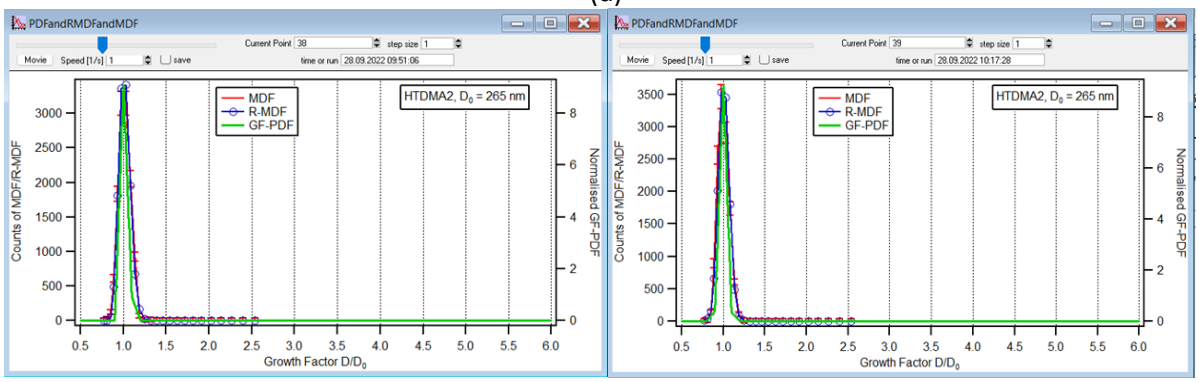

(e) (f)

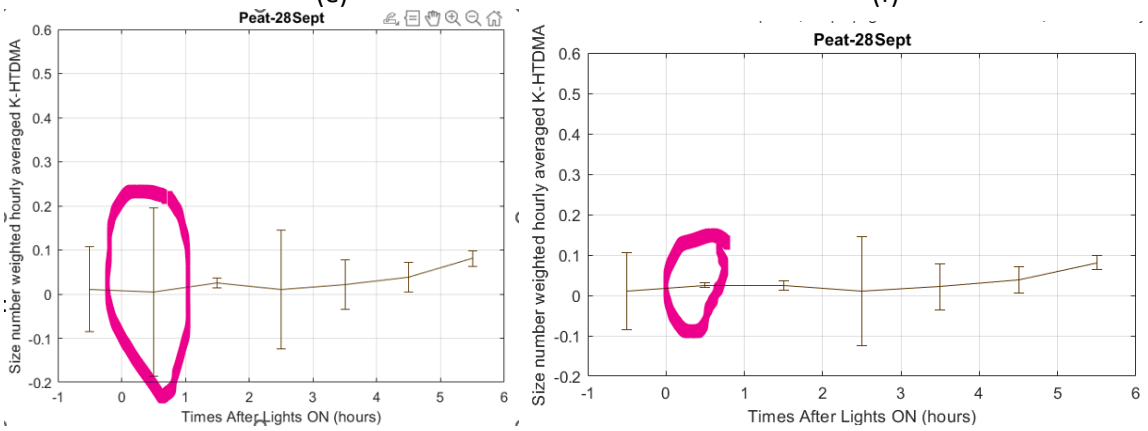

(g) (h)

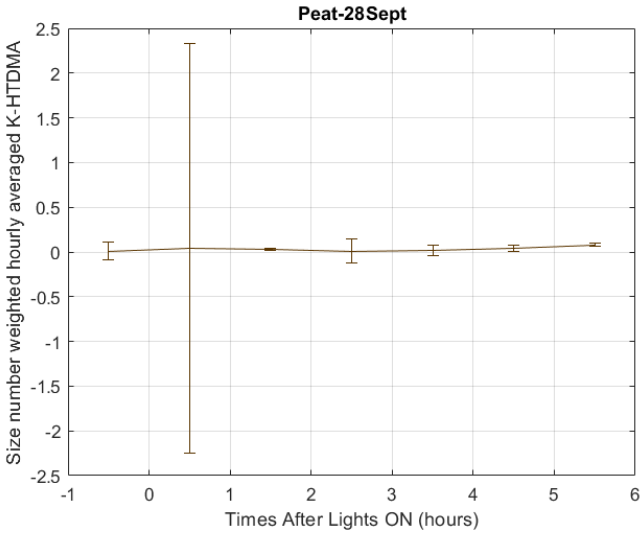

(i)

Figure S5. Investigation of a mean point with a large value of propagated error. **a**) The propagated error with high value; **b**) and **c**) Manual Check for points that have large averaged time point error; Results: the two points at a size of 265 nm measured for a 1-hour period before the lights were turned on in c) Both have the highest average time point error and the lowest time point derived kappa values. **d**) Comparison of both time point kappa values and time point errors of 265 nm particles during different periods. **e**) Initial graphs before investigation. **f**) The reproduced graph when the two points in c) are removed. Even though removing the two points greatly reduces the propagated errors from g) to h), this was not applied because there was no unusual appearance in the fitting graphs (just like the graphs of other data points) or a low particle concentration issue, so it's likely appropriate to consider them as valid data points. Removing only the point with a negative value (-0.0176) even further results in a much larger propagated error (**i**)

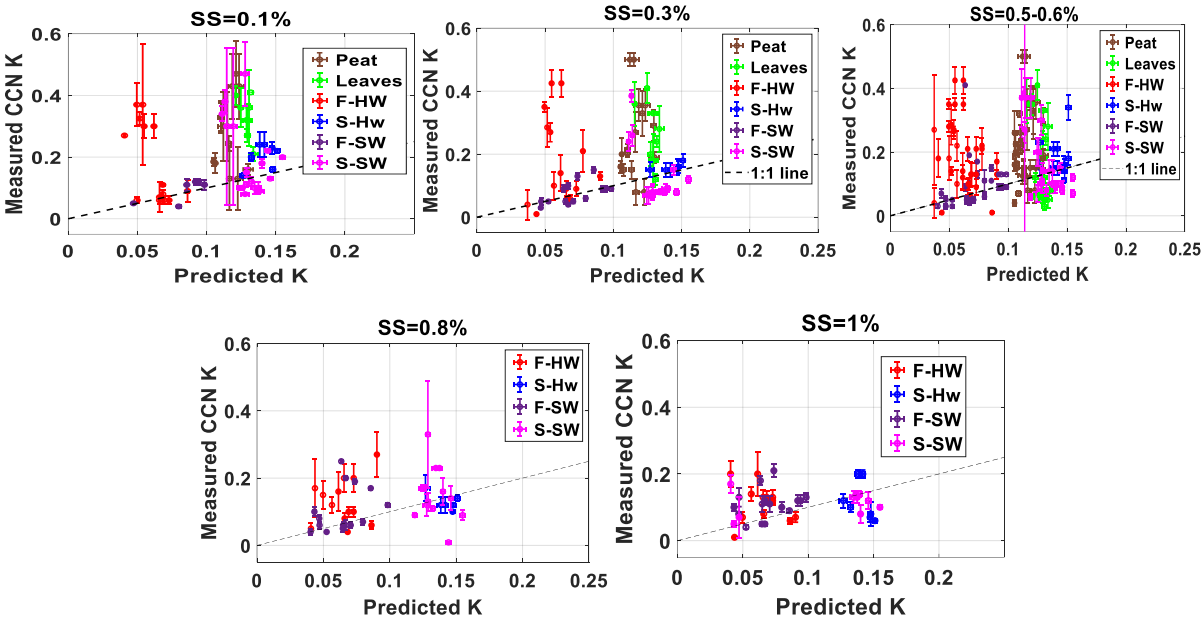

(a)

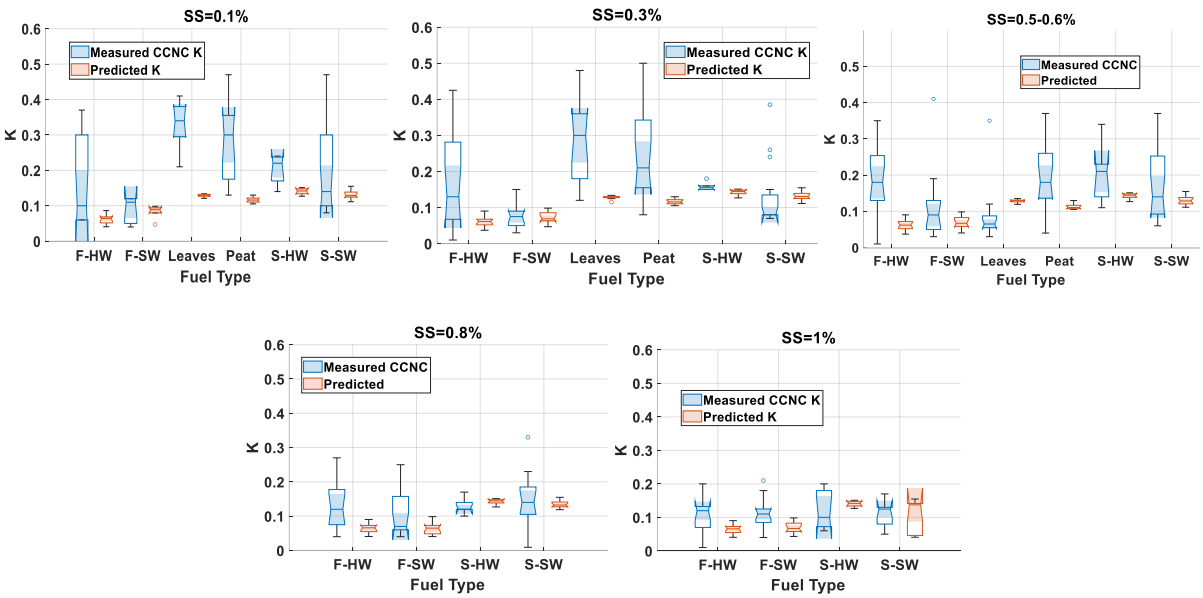

(b)

Figures S6 SS separated plots of the Predicted versus Measured CCNC scatter plots (a) and Predicted versus Measured CCNC data distribution box-whisker plots (b). Each point reflects hourly mean value with error bar represent propagated errors.

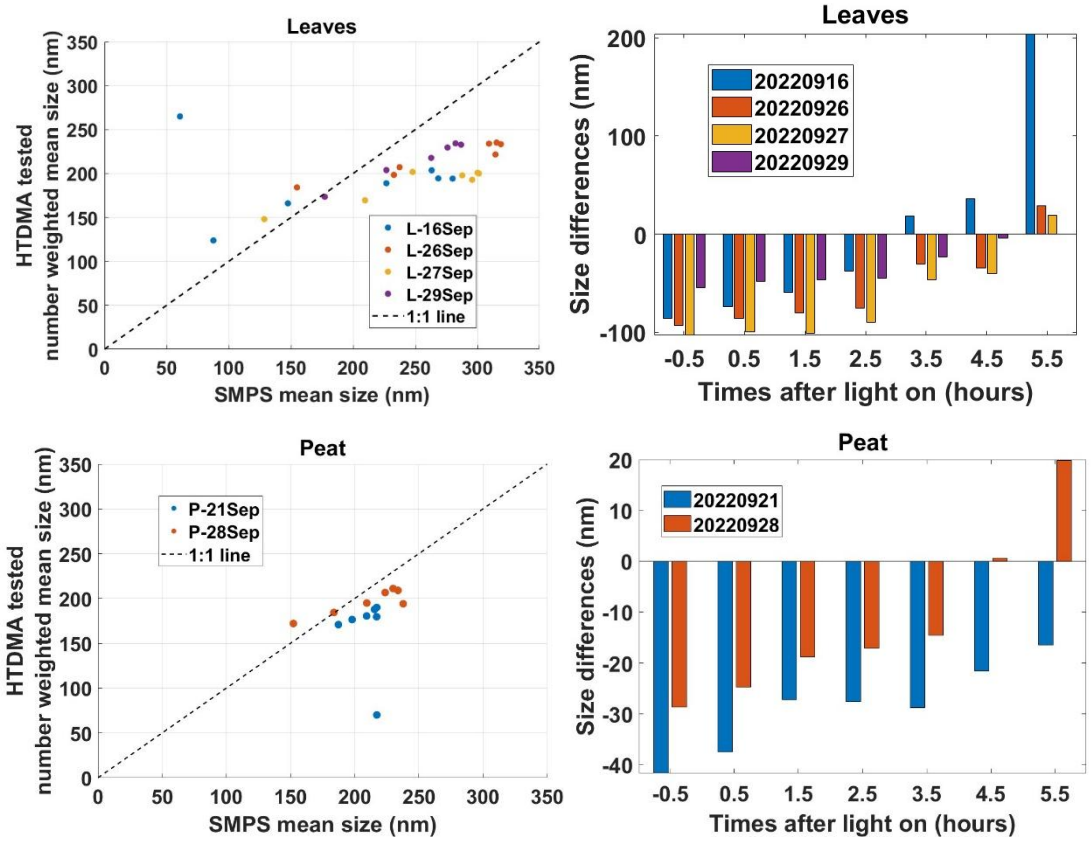

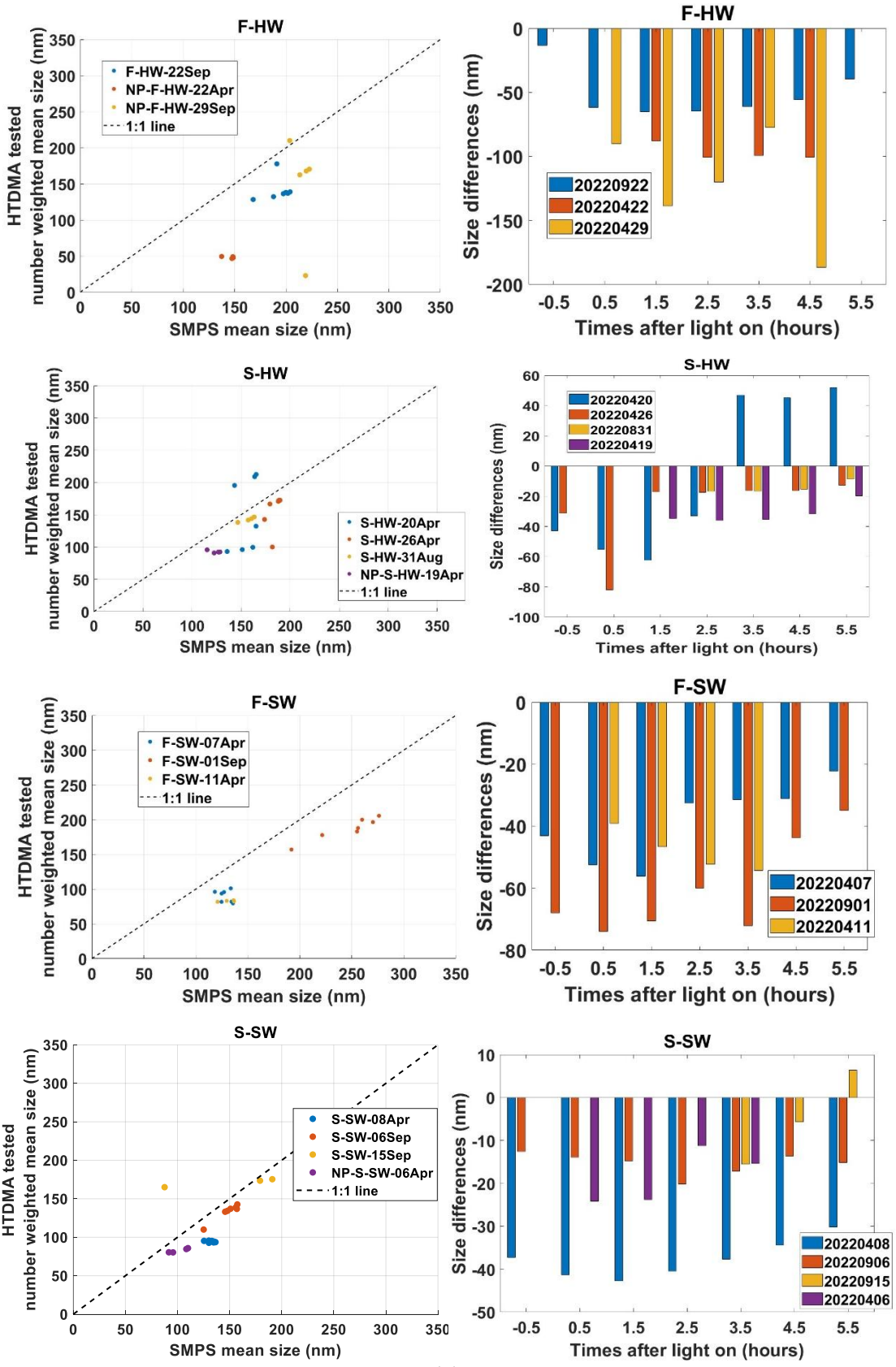
F-HW
HTDMA tested number weighted mean size (nm)
SMPS mean size (nm)
F-HW-22Sep
NP-F-HW-22Apr
NP-F-HW-29Sep
1:1 line
F-HW
Size differences (nm)
Times after light on (hours)
20220922
20220422
20220429
S-HW
S-HW-20Apr
S-HW-26Apr
S-HW-31Aug
NP-S-HW-19Apr
1:1 line
S-HW
20220420
20220426
20220831
20220419
F-SW
F-SW-07Apr
F-SW-01Sep
F-SW-11Apr
1:1 line
F-SW
20220407
20220901
20220411
S-SW
S-SW-08Apr
S-SW-06Sep
S-SW-15Sep
NP-S-SW-06Apr
1:1 line
S-SW
20220408
20220906
20220915
20220406

(a)

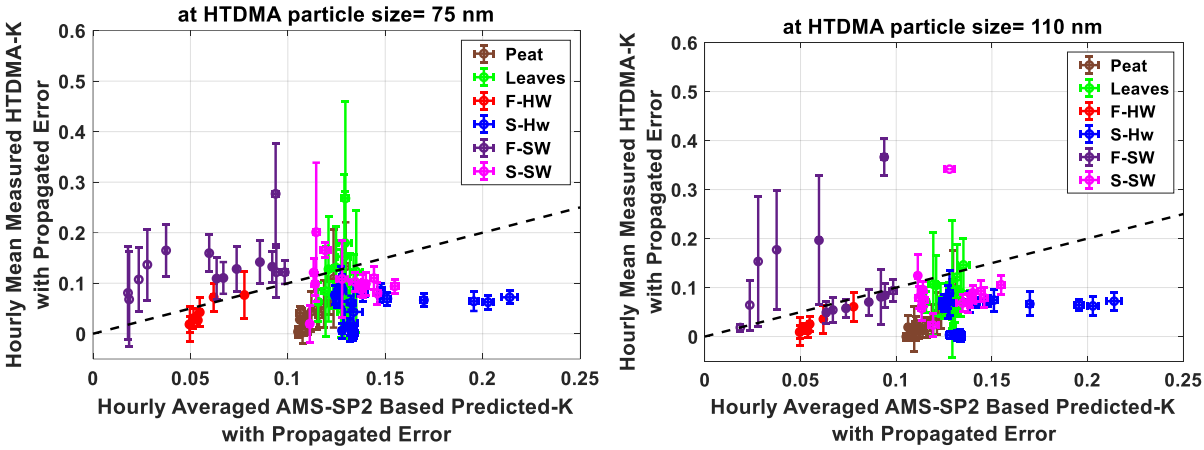

(**b**)

Figure S7. a) (Left) HTDMA tested number-weighted (NW) mean sizes Versus SMPS number mean size; (Right) Time Series' Discrepancy Values of HTDMA tested NW-mean size Subtracted By SMPS number mean size; **b**) Size Dependence HTDMA Measured κ versus Composition-Based Predicted κ: (Left) at HTDMA tested size of 75 nm; (Right) at HTDMA tested size of 110 nm

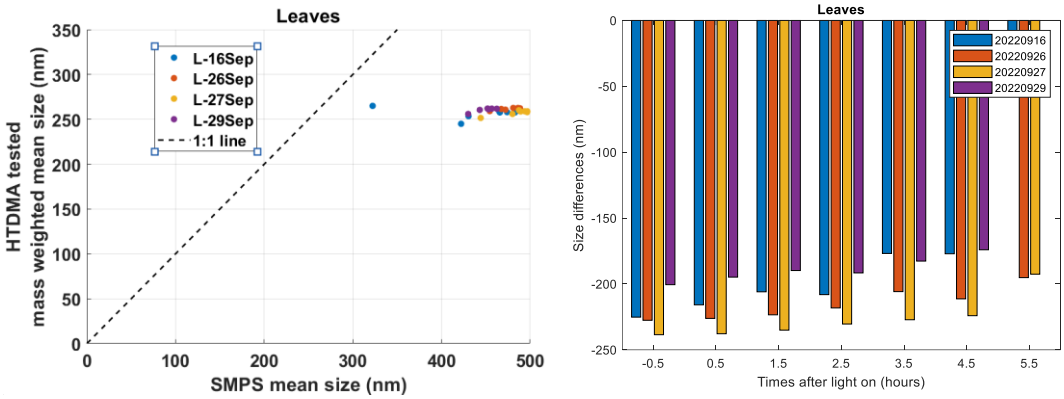

(a) (b)

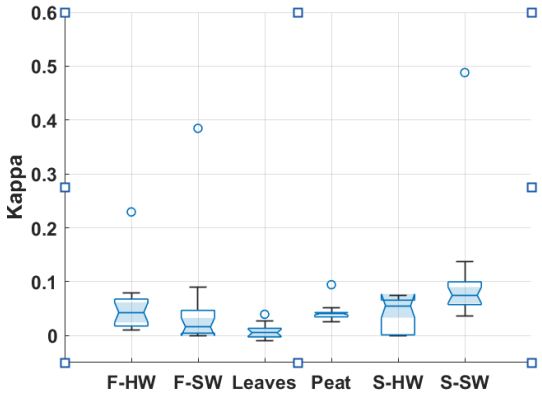

(c)

Figure S8. HTDMA tested mass-weighted (MW) mean sizes Versus SMPS number mean size of Leaves Experiments (**a**); Time Series' Discrepancy Values of HTDMA tested MW-

mean size Subtracted By SMPS number mean size (**b**); Whisker-and-Box Plot Chart of HTDMA mass-weighted (MW) mean κ values distribution (**c**)

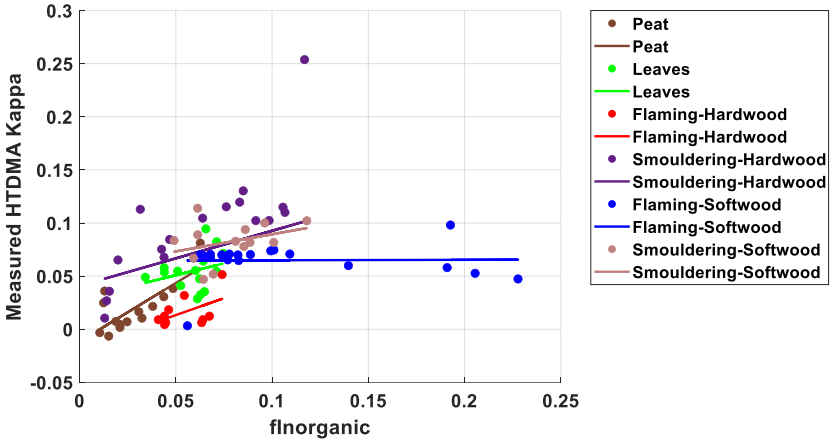

(**a**)

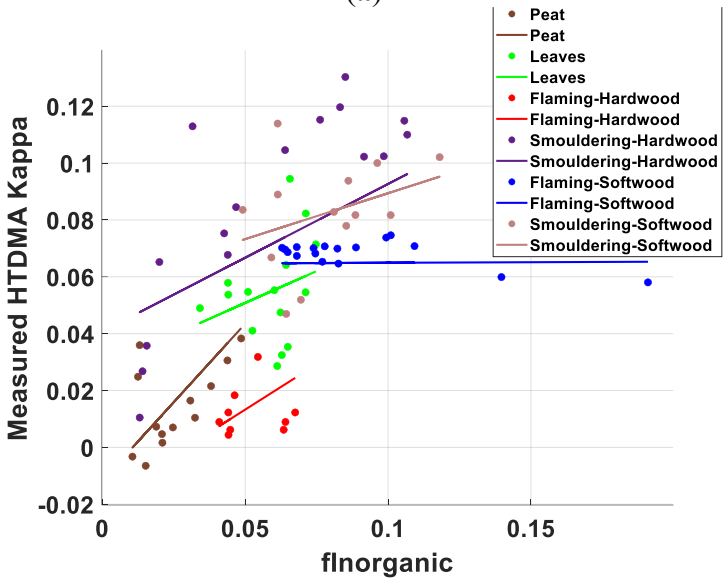

Figure S9. Linear regression analysis - Organic and inorganic κ revealed, with all data points (a); Linear regression analysis - Organic and inorganic κ revealed, with the box-and-whisker plot-detected outliers of the peat experiment, flaming hardwood (b)

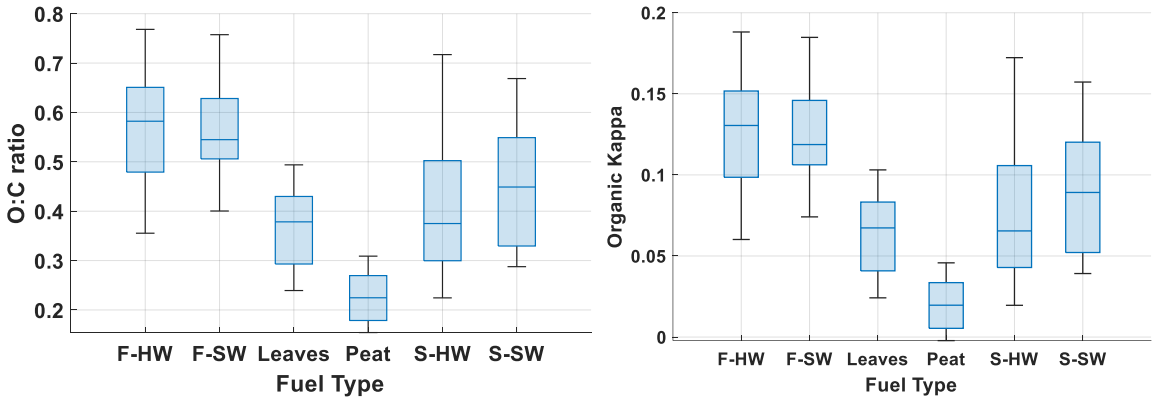

Figure S10. Whisker-and-Box Plot Chart of AMS-f44 Derived O:C Ratio Values of Each Experiment Type a); Whisker-and-Box Plot Chart of O:C Ratio-Based Calculated Organic κ (κ_{org}) Values of Each Experiment Type b)

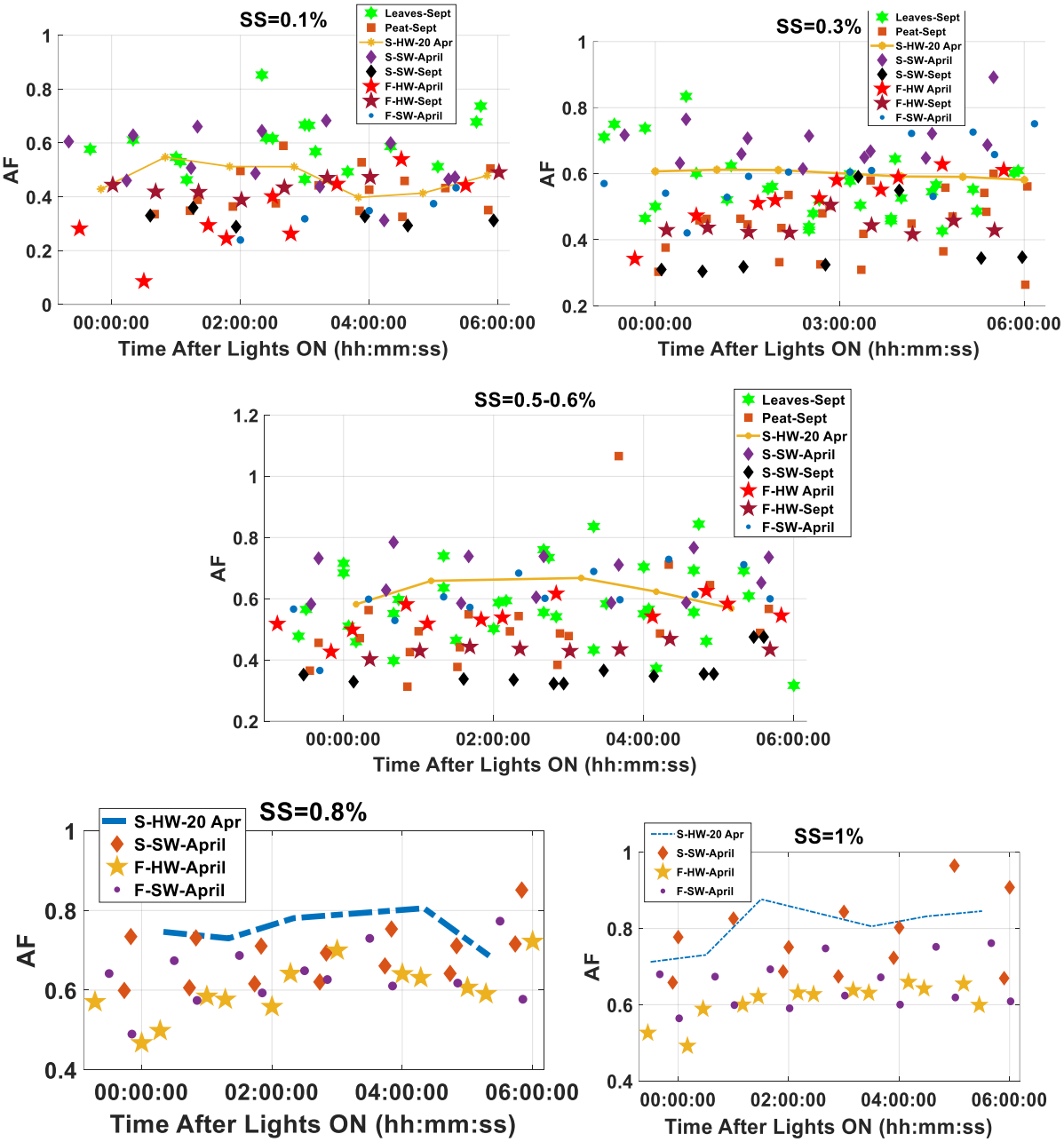

Figure S11. Time Series CCNc Activation Fraction (AF) Graphs of All Photoageing Experiments at Each SuperSaturation (SS)

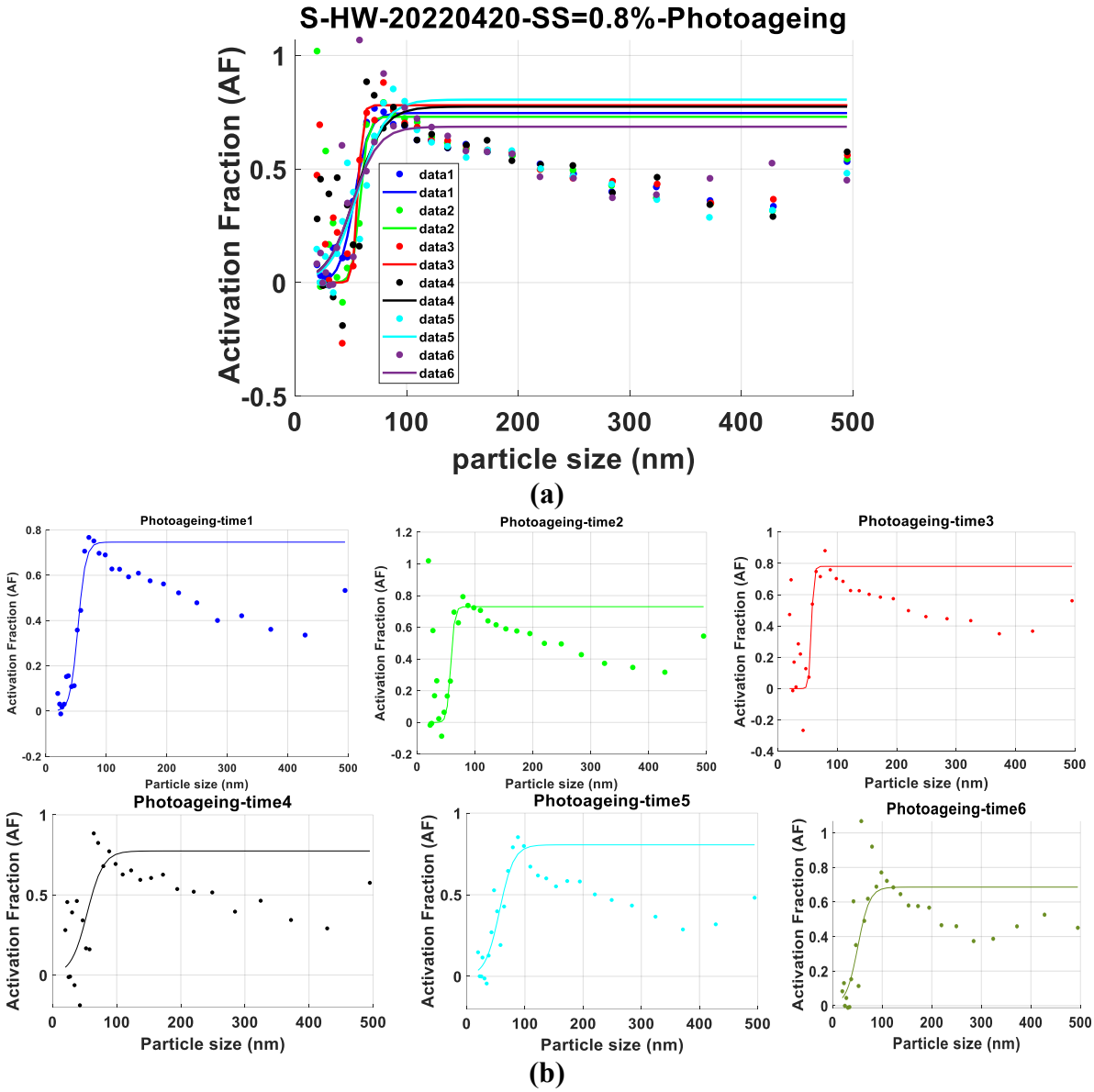

Figures S12 Examples of the CCNC Activation Fraction (AF) Curve Fittings: Joined (a) and Separated (b)

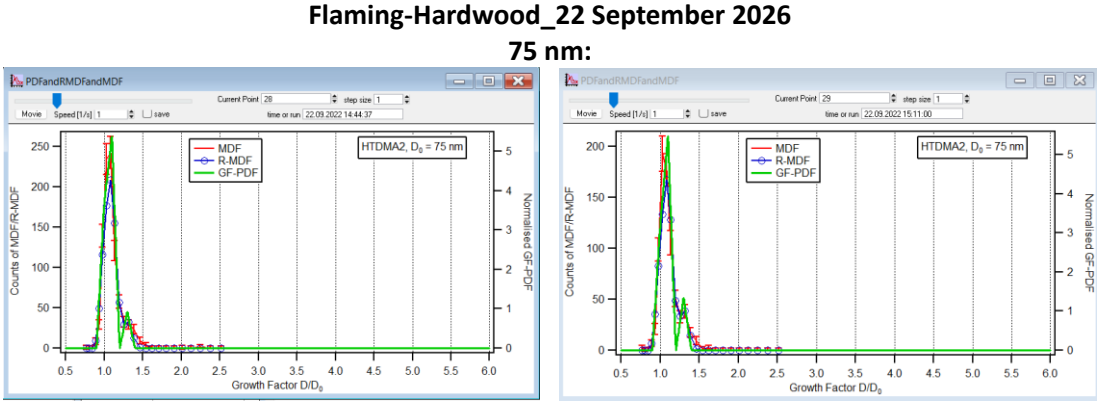

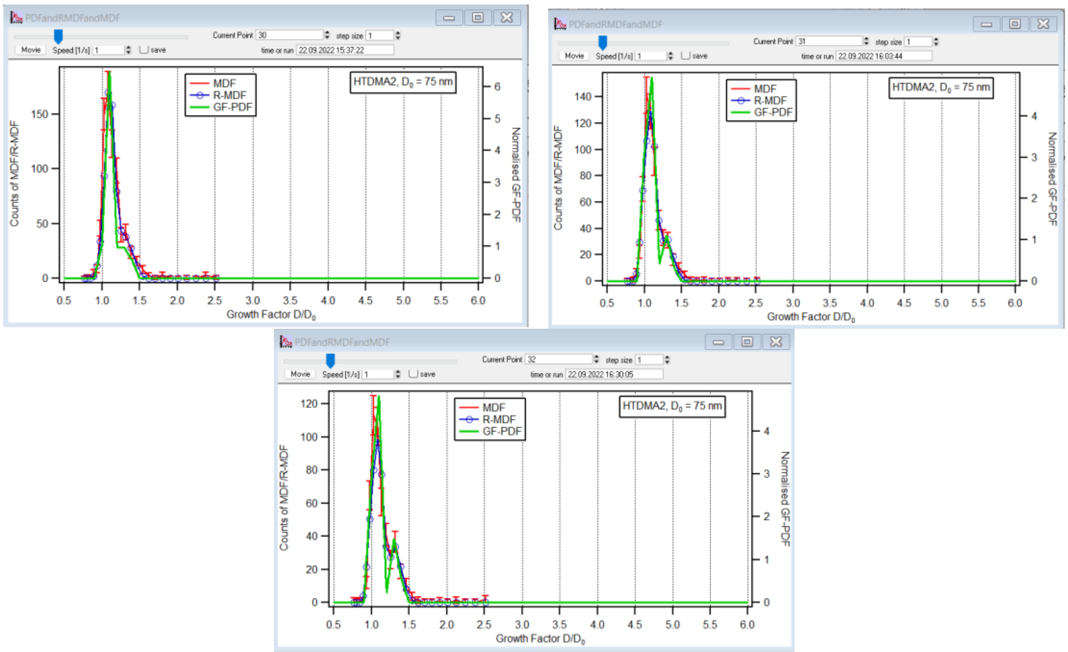
PDFandRMDFandMDF
HTDMA2, D0 = 75 nm
MDF
R-MDF
GF-PDF
Counts of MDF/R-MDF
Normalised GF-PDF
Growth Factor D/D0

110 nm:

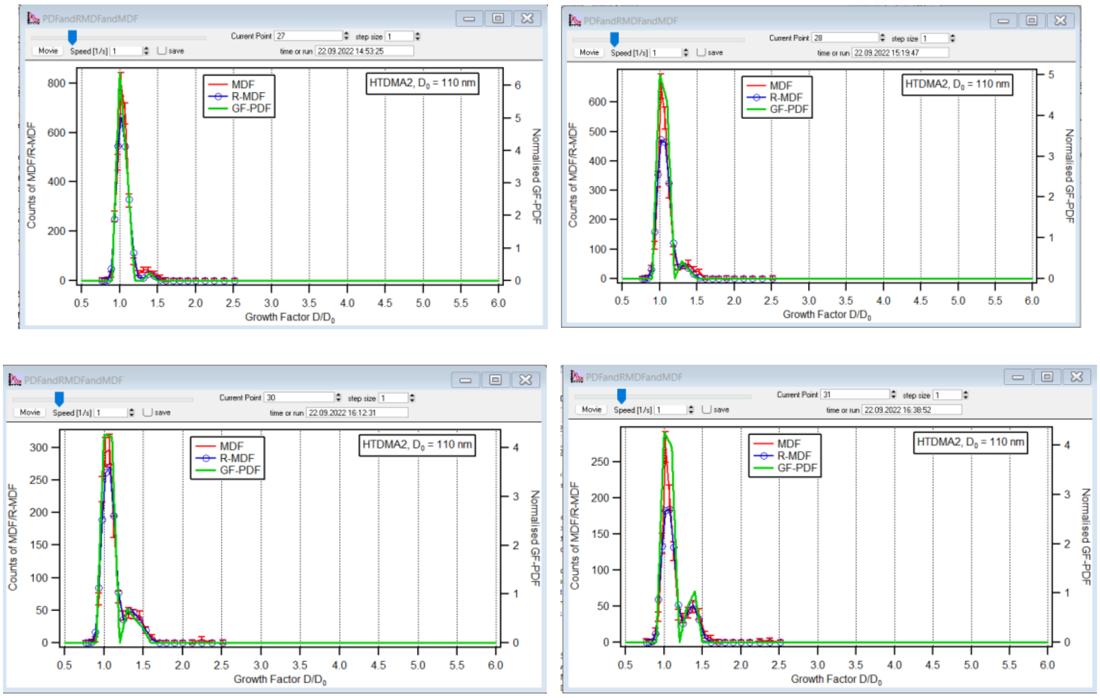
PDFandRMDFandMDF
HTDMA2, D0 = 110 nm
MDF
R-MDF
GF-PDF
Counts of MDF/R-MDF
Normalised GF-PDF
Growth Factor D/D0

165 nm:

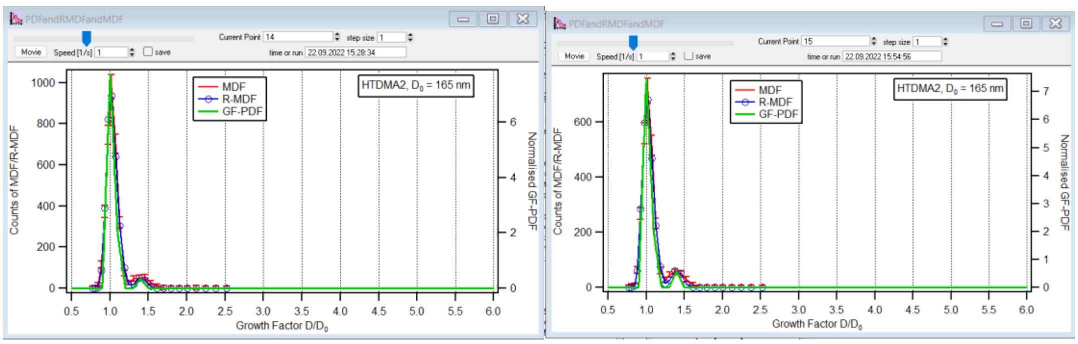
PDFandRMDFandMDF
HTDMA2, D0 = 165 nm
MDF
R-MDF
GF-PDF
Counts of MDF/R-MDF
Normalised GF-PDF
Growth Factor D/D0

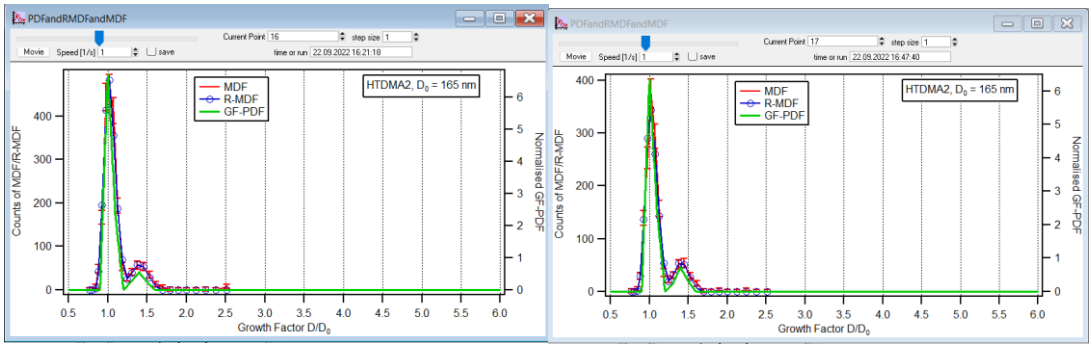

Smouldering-Hardwood_31 August 2026 (75 nm, 110 nm, 265 nm)

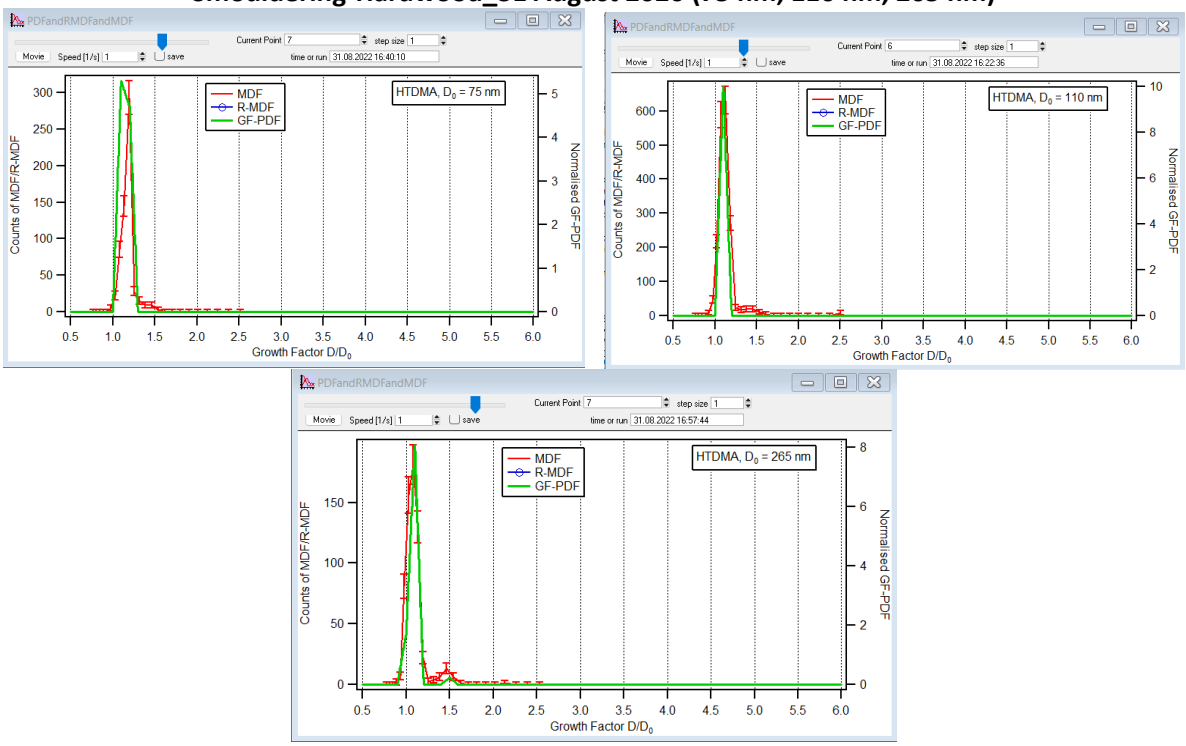

Figure S13 Example of HTDMA graphs Comparison between Flaming Hardwood and Smouldering Hardwood. Two peaks started to appear in the last several hours of the photo-ageing period in the Flaming Hardwood experiment – slightly lower growth factor (GF at around one) of the 1st peaks at larger particle sizes; the Smouldering-Hardwood experiment tends to preserve the one-peak-only appearance during the whole photo-ageing experiment at Growth Factor (GF) values slightly larger than one at all particle sizes.

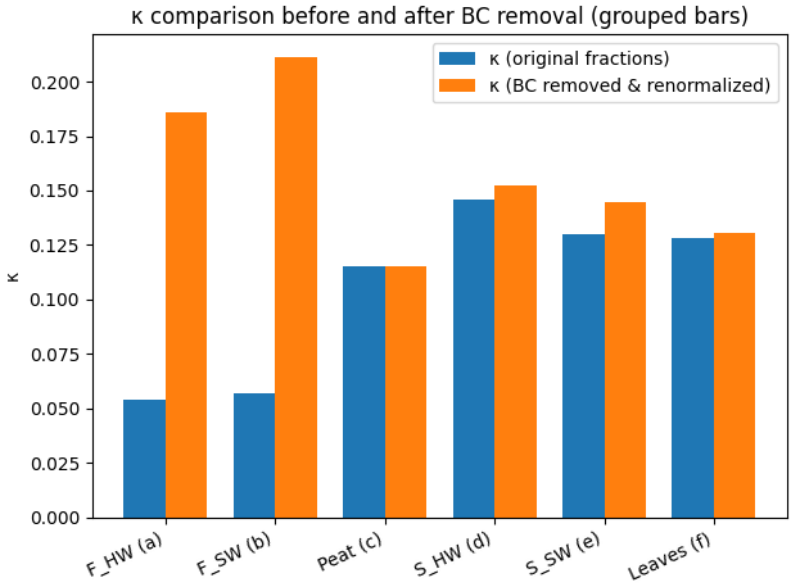

Figure S14 Comparison of the mean k predicted values using the mass fractions that include BC versus those that do not include BC.

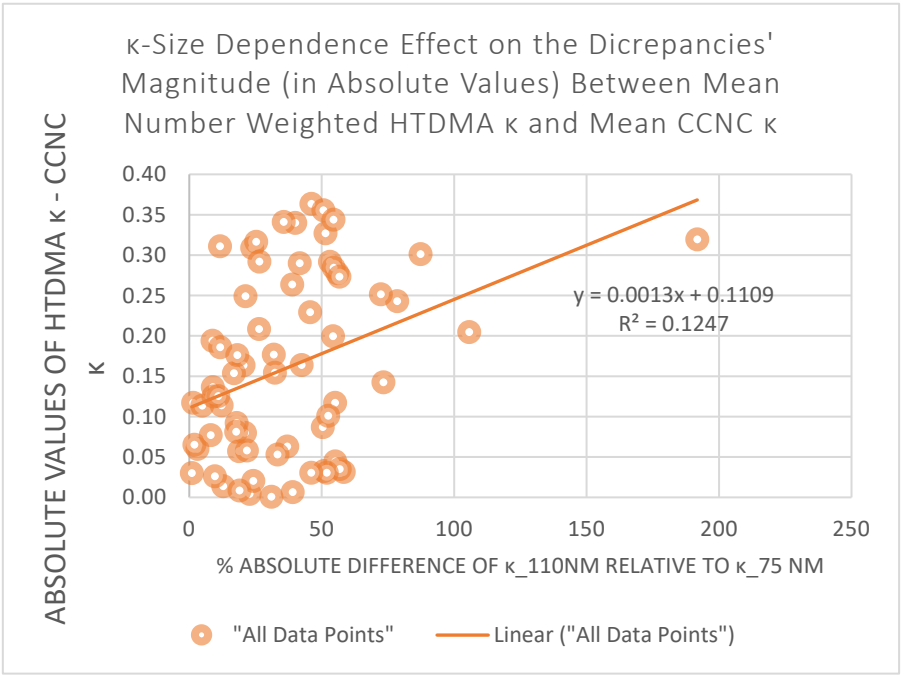

(a)

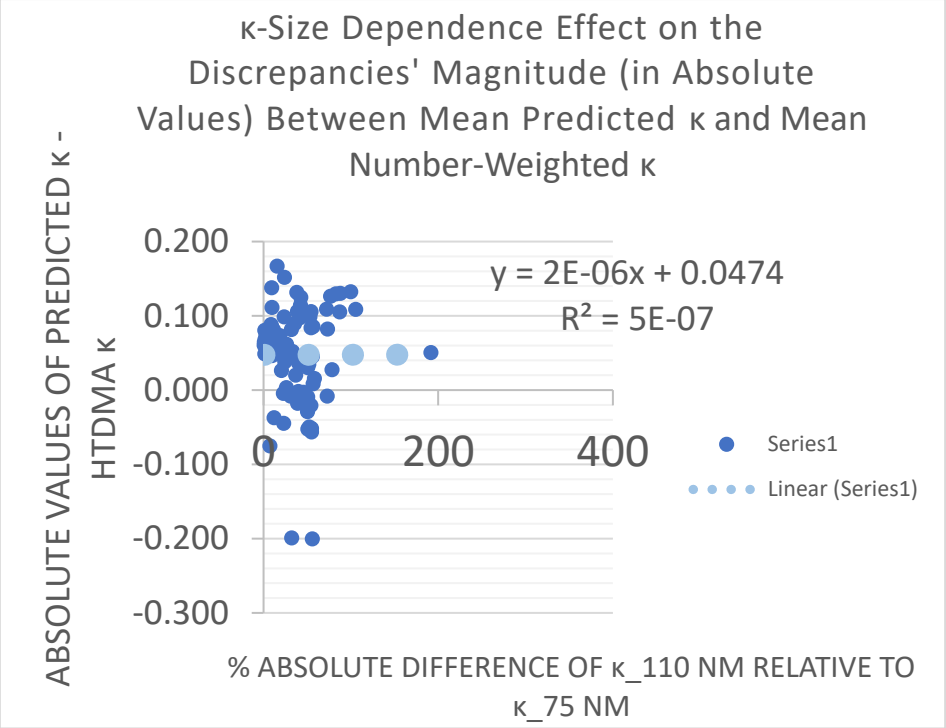

(b)

Figure S16 Investigation on the Effect of Hygroscopicity Size Dependence